

Control of an Electric Vehicle Powertrain to Mitigate Shunt and Shuffle

Master's thesis in Automotive Engineering

VICTOR HERMANSSON & KEDARNATH MOPARTHI

MASTER'S THESIS IN AUTOMOTIVE ENGINEERING

Control of an Electric Vehicle Powertrain to Mitigate Shunt and Shuffle

VICTOR HERMANSSON & KEDARNATH MOPARTHI

Department of Signals and Systems
Division of Automatic control, Automation and Mechatronics
CHALMERS UNIVERSITY OF TECHNOLOGY
Göteborg, Sweden 2016

Control of an Electric Vehicle Powertrain to Mitigate Shunt and Shuffle

VICTOR HERMANSSON & KEDARNATH MOPARTHI

© VICTOR HERMANSSON & KEDARNATH MOPARTHI, 2016-06-01

Master's Thesis EX056/2016

ISSN 1652-8557

Department of Signals and Systems

Division of Automatic control, Automation and Mechatronics

Chalmers University of Technology

SE-412 96 Göteborg

Sweden

Telephone: + 46 (0)31-772 1000

Cover:

Outline of the controlled electric powertrain model used for simulation.

Department of Signals and Systems

Göteborg, Sweden 2016-06-01

Control of an Electric Vehicle Powertrain to Mitigate Shunt and Shuffle

Master's thesis in Automotive Engineering

VICTOR HERMANSSON & KEDARNATH MOPARTHI

Department of Signals and Systems

Division of Automatic control, Automation and Mechatronics

Chalmers University of Technology

Abstract

Automotive industry is moving towards electric propulsion. With new technology comes new problems to solve. To be competitive in this fast paced industry every detail needs to be addressed for better driveability, comfort and improved component life, which consumers can easily relate to as premium feel. One issue which can deteriorate all the before mentioned characteristics is oscillations in the driveline. The fast response from the electric motor and poor damping in the driveshaft material gives rise to torsional oscillations which in turn translates into jerk in the vehicle motion. This low frequency phenomenon is known as shuffle representing the first resonance peak in the driveline.

By implementing an active controller which regulates the torque demand to the electric motor it is seen that the shuffle phenomenon can be considerably reduced, thus bringing the driveline to a steady state quickly for smoother drive. Two alternate control strategies were used for this and compared against each other for performance differences. Also, in the later stage, backlash was introduced into the plant model to study the effect on the controls from nonlinearities within the system. In the same process a study was done on the effect on the powertrain housing oscillations due to the shaft oscillations and vice versa in two cases each, one being without any active damping and the other with active damping, as powertrain housing oscillations are in a sense dynamic backlash.

The two linear control strategies used for this study showed promising capability for actively damping the oscillations. But when introduced to non-linearities they could not provide with optimal control, so an extra control strategy was implemented to overcome this. Furthermore the study involving powertrain housing oscillations showed that, by implementing active damping control for the driveline the housing oscillations can be reduced as well, which in turn could aid in optimizing the powertrain housing mounts.

Keywords: shuffle, shunt, driveline oscillations, virtual physical damper, LQR, LQRY, estimator, backlash, powertrain housing

Reglering av en elektrisk fordonsdrivlina för att motverka ryck och oscillationer
Examensarbete inom Fordonsteknik
VICTOR HERMANSSON & KEDARNATH MOPARTHI
Institutionen för Signaler och system
Avdelningen för Reglerteknik, Automation och Mekatronik
Chalmers tekniska högskola

Sammanfattning

Fordonsindustrin rör sig mer och mer mot elektrisk framdrivning. Med ny teknik kommer nya problem att lösas. För att vara konkurrenskraftig i denna snabbväxande industri måste varje detalj bearbetas i syfte att förbättra körbarhet, komfort och komponentlivslängd, egenskaper som konsumenter lätt kan relatera till som premiumkänsla. Ett problem som kan försämra alla tidigare nämnda egenskaper är oscillationer i drivlinan. Den snabba responsen hos den elektriska motorn och den svaga dämpningen i drivaxelns material ger upphov till torsionssvängningar vilket i sin tur leder till ryck i fordonets rörelse. Detta lågfrekvensfenomen är i den engelskspråkiga litteraturen känt som shuffle, och representerar den första resonanstopp i drivlinan.

Genom att implementera en regulator som reglerar efterfrågat vridmoment till elmotorn, framgår det av rapporten att shuffle-fenomenet kan minskas avsevärt, vilket stabiliserar drivlinan snabbare och ger fordonet en mjukare gång. Två alternativa reglerstrategier användes för detta och jämfördes mot varandra för att skildra prestandaskillnader. I ett senare skede infördes dödgång i drivlinemodellen för att studera påverkan på regleringen från olinjäriteter i systemet. En studie utfördes också på påverkan på drivlinehusets oscillationer orsakade av drivaxeloscillationerna och vice versa i två fall vardera, det första utan någon aktiv dämpning och det andra med aktiv dämpning, eftersom drivlineoscillationer på sätt och vis är dynamisk dödgång.

De två linjära reglerstrategierna som användes i den här studien visade på lovande kapacitet att aktivt dämpa oscillationerna. Men när de utsattes för olinjäriteter kunde de inte leverera en optimal reglering, varför en extra reglerstrategi implementerades för att överkomma detta. Vidare visade studien innehållande drivlinehusoscillationer att, genom att implementera aktiv dämpningsreglering av drivlinan, kunde drivlinehusoscillationerna också reduceras, vilket i sin tur skulle kunna bidra till att optimera drivlinehusets infästningar.

Nyckelord: ryck, drivlineoscillationer, virtuell fysisk dämpare, LQR, LQRY, observatör, dödgång, drivlinehus

Preface

National Electric Vehicle Sweden AB is moving forward with the vision to shape mobility for a more sustainable future. In this process the company is extensively working hard to create its mark with electric vehicles and leaving no detail unaddressed. Along the way it was noticed that the two phenomenon called shuffle and shunt could influence the ride quality of the vehicle. On further literature review it became evident that shuffle and shunt result in first eigen frequencies in the range which can be felt by humans, therefore it is necessary to focus on mitigating these effects for improved driveability and comfort.

Acknowledgement

Firstly we would like to thank National Electric Vehicle Sweden AB for providing us an opportunity to work on real world problem as our Master thesis. A special thanks to our examiner Jonas Fredriksson, Associate Professor at Signals and Systems at Chalmers, and Olle Johansson, supervisor at National Electric Vehicle Sweden AB, for their continuous guidance and the valuable support they have been providing us for the thesis. The immense support and interest from a number of people who helped this project by providing crucial inputs is highly appreciated. We would also like to extend our acknowledgment to fellow Master thesis students Karl-Johan Hagelin and Robert Samefors for being a wonderful company throughout the thesis.

Göteborg March 2016-06-01

VICTOR HERMANSSON & KEDARNATH MOPARTHI

Notations

Roman upper case letters

A	Frontal area of the vehicle
C_h	Damping coefficient of powertrain housing mounts
C_s	Damping coefficient of driveshaft
F_{air}	Air resistance
F_g	Gradient resistance
F_{res}	Longitudinal wheel resistance
F_{rf}	Longitudinal tyre force at rear tyres
F_{trac}	Traction force
F_{xf}	Longitudinal tyre force at front tyres
$F_{xf,eff}$	Effective longitudinal tyre force at front tyres
$F_{rf,eff}$	Effective longitudinal tyre force at rear tyres
F_{zf}	Normal tyre force at front tyres
F_{zr}	Normal tyre force at rear tyres
J_e	Lumped gearbox inertia
J_h	Inertia of powertrain housing
J_m	Motor inertia
J_1	Inertia of input shaft in gearbox
J_2	Inertia of intermediate shaft in gearbox
J_3	Inertia of output shaft in gearbox
K_h	Stiffness of powertrain housing mounts
K_s	Stiffness of driveshaft
Q_{LQR}	Weighting matrix for states penalising
Q_{LQRY}	Weighting matrix for output states penalising
R_{xf}	Longitudinal rolling resistance at front tyres

R_{xr}	Longitudinal rolling resistance at rear tyres
R_{LQR}	Weighting matrix for control signal penalising
R_{LQRY}	Weighting matrix for control signal penalising
T_g	Driveshaft torque
T_m	Motor input torque
$T_{resistance}$	Resistance torque
T_{trac}	Traction torque
T_1	Torque output from motor
V	Covariance matrix for sensor signals
W	Covariance matrix for estimator process signals

Roman lower case letters

a_v	Vehicle longitudinal acceleration
c_w	Drag coefficient
g	Gravitational acceleration
h	Height of centre of gravity
h_{air}	Height of centre of pressure
i	Effective gear ratio
i_1	First stage gear ratio
i_2	Second stage gear ratio
l_f	Longitudnal distance of front axle from centre of gravity
l_r	Longitudnal distance of rear axle from centre of gravity
m_v	Mass of vehicle
r	Wheel radius
r_e	Effective wheel radius
v_v	Vehicle longitudinal speed

Greek letters

α	Road gradient
θ_b	Backlash angular position
θ_c	Effective angular position due to backlash
θ_g	Gearbox output angular position
θ_m	Motor angular position
θ_w	Wheel angular position
ρ	Air density
φ	Half of deadband
ω_b	Backlash angular speed
ω_g	Gearbox output angular speed
$\dot{\omega}_g$	Gearbox output angular acceleration
ω_{g2}	Effective angular speed due to powertrain housing
$\dot{\omega}_{g2}$	Effective angular acceleration due to powertrain housing
ω_h	Powertrain housing angular speed
$\dot{\omega}_h$	Powertrain housing angular acceleration
ω_m	Motor angular speed
$\dot{\omega}_m$	Motor angular acceleration
ω_w	Wheel angular speed
$\dot{\omega}_w$	Wheel angular acceleration

Abbreviations

CoG	Centre of gravity
CoP	Centre of pressure
EM	Electric motor
GB	Gearbox
LQR	Linear Quadratic Regulator
LQRY	State-output Linear Quadratic Regulator
PT	Powertrain

Contents

Abstract.....	I
Sammanfattning.....	III
Preface.....	V
Acknowledgement.....	VII
Notations.....	IX
Abbreviations.....	XIII
Contents.....	XV
1 Introduction.....	1
1.1 Background.....	1
1.2 Problem Statement.....	1
1.3 Goals.....	1
1.4 Method.....	2
1.5 Limitations.....	2
1.6 Main Contributions.....	2
1.7 Outline of the Thesis.....	3
2 Theory.....	4
2.1 Driveline Stabilization Issue.....	4
2.2 Mechanics and Dynamics.....	4
2.3 Vehicle Dynamics.....	4
2.3.1 Longitudinal Tyre Force.....	5
2.3.2 Rolling Resistance.....	8
2.3.3 Air Resistance.....	9
2.3.4 Gradient Resistance.....	9
2.4 Backlash.....	9
2.4.1 Backlash Modelling.....	10
2.5 Wheel Speed Sensor.....	12
2.6 LQR.....	12
2.6.1 State LQR Optimal Problem:.....	13
2.6.2 State-output LQR (LQRY) Optimal Problem:.....	13
2.7 LQ Estimator.....	14
3 Modelling.....	16
3.1 Making of the Powertrain and Vehicle Model.....	16
3.1.1 Electric Motor.....	16
3.1.2 Gearbox.....	17
3.1.3 Powertrain Housing.....	19

3.1.4	Driveshaft.....	20
3.1.5	Wheel.....	20
3.2	State Space Model.....	22
3.3	Simulink Model.....	24
3.3.1	Electric Motor and Gearbox.....	24
3.3.2	Power Saturation.....	24
3.3.3	PT Housing.....	25
3.3.4	Backlash.....	25
3.3.5	Driveshaft.....	25
3.3.6	Wheel.....	26
3.3.7	Tyre.....	26
3.3.8	Vehicle Body.....	27
4	Control Design.....	28
4.1	Virtual Physical Damper.....	29
4.2	LQ Estimator.....	29
4.3	LQR.....	30
4.4	LQRY.....	30
4.5	Controller Torque Saturation.....	31
4.6	Backlash Estimation.....	31
4.6.1	Contact Mode.....	32
4.6.2	Non-contact Mode.....	33
4.7	Backlash Controller.....	34
5	Simulations.....	35
5.1	Frequency Response Plots for State Space Model.....	35
5.2	Plant Model.....	36
5.3	Powertrain Model with Virtual Physical Damper.....	37
5.4	Virtual Physical Damper Using Wheel Speed Sensor.....	39
5.5	Checking for Possibility of Improvement in Physical Damper by Varying Controller Damping Value.....	40
5.6	Implementing Estimator.....	41
5.7	Performance Comparison of Physical Damper with Sensor and Estimator.....	43
5.8	Comparison of Estimators of Two Different Approaches.....	44
5.9	Robustness Analysis of Estimator.....	46
5.9.1	Vehicle Mass.....	47
5.9.2	Shaft Stiffness.....	48
5.9.3	Motor Inertia.....	49

5.10	Powertrain Model with LQR Controller	50
5.11	Powertrain Model with LQRY Controller	51
5.12	Performance Comparison of Physical Damper with Estimator, LQR and LQRY.....	51
5.13	Robustness Analysis of Virtual Physical Damper and LQRY with Estimator.....	53
5.13.1	Vehicle Mass.....	53
5.13.2	Shaft Stiffness	54
5.13.3	Motor Inertia.....	55
5.14	Effect from Backlash in the Model.....	56
5.15	Torque Saturation.....	58
5.16	Effect of Backlash Controller for Various Controllers	59
5.17	Effect Due to and on Powertrain Housing Oscillations	62
5.17.1	Effect on the Shaft Oscillations Due to Housing Oscillations.....	62
5.17.2	Effect on the Housing Oscillations Due to Shaft Oscillations	63
5.18	Controller Performance for Different Torque Input Levels.....	64
5.19	Backlash Estimation	65
6	Conclusions.....	67
7	Future Work Recommendations.....	69
	References.....	70
	Appendix.....	i
	Appendix I: Vehicle Parameters.....	i
	Appendix II: Simulink Model.....	iii

1 Introduction

This chapter introduces the reader to the thesis report. It provides a background to and description of the problems the thesis aims to solve, while it also presents a review of previous publications within the field and states the contributions of the work.

1.1 Background

To be ahead of the game in the highly dynamic automotive industry it is important to develop and maintain a satisfied patronage by working on the details and inevitably uplifting the premium feel for the product. It is also important to work on such details as they aid in understanding the system in a better way and that knowledge can be used for developing controlled systems that are faster and more efficient.

As the electric powertrain has quicker response time and lesser mechanical damping compared to a conventional powertrain with internal combustion engine, torsional oscillations are generated at the driveshaft due to its elasticity which is termed as driveline shuffle. The nonlinearities like backlash, when introduced, leads to higher gear contact forces and a momentary acceleration of the driveline, an unwanted phenomenon known as shunt. This thesis focuses on developing a control strategy to actively damp the driveline shuffle and also study the impact of backlash on the performance of the system.

Previous works presented on the topic confirm that driveline oscillation is an issue influencing the driveability. In [1] it was stated that driveability influence can be felt in a frequency range of 0-40 Hz. For electric powertrains the first eigen frequency typically shows up below 10 Hz, see [1], [2], [3] and [4], meaning that it is important to address driveline oscillations for an improved driveability. In [5], concerns were also expressed on presence of backlash as a nonlinearity, which will degrade the driveability and effect the control system performance making it an interesting topic to study.

1.2 Problem Statement

The oscillations occurring in the electric powertrain due to driveshaft flexibility and backlash causes uncomfortable jerking of the vehicle and results in high gear contact forces. To mitigate this the driveline needs to be actively stabilized by controlling the torque of the electric motor.

1.3 Goals

The goals of the thesis work is to:

- Develop a reference control system imitating a simple virtual physical damper.
- Develop a better performing control system that stabilizes the driveline oscillations.

- Investigate the influence of backlash on the dynamics of the system and develop a control system to mitigate the same.
- Eliminate issues due to wheel speed measurement and CAN transport delay.
- Develop driveshaft torque estimation.

1.4 Method

The thesis work has been carried out according to the procedure presented in the following points and in the same order:

1. Modelling of the electric powertrain (PT), vehicle body, wheels and tyres necessary to replicate the shuffle.
2. Design of a reference controller imitating a simple virtual physical damper.
3. Design of an improved stabilization control to reduce gain torque loss.
4. Comparison of performance of improved control with that of simple physical damper.
5. Study of the effect from the backlash on the controller performance.
6. Study of the impact by driveshaft oscillations on powertrain housing oscillations and vice versa with and without active damping.

1.5 Limitations

The thesis work has been limited to the following constraints:

- All the research and development carried out within the thesis work is limited to simulation environment.
- Only longitudinal dynamics of the vehicle is considered.
- No parameter identification has been done for a specific vehicle.

1.6 Main Contributions

The thesis work adds value of interest to the field that has not been investigated, or at least not found by the authors when reviewing the literature in the field. The following points are the main contributions of the work:

- Investigation of the impact by driveshaft oscillations on powertrain housing and vice versa with and without active damping, and the effects of changing the characteristics of the powertrain housing mounts.

- Investigation of the use of state-output linear quadratic regulator control (LQRY).
- Investigation of prospects of improvement of virtual physical damper performance by using a wheel speed estimator.

1.7 Outline of the Thesis

The report is divided into six main chapters: Theory, Modelling, Control Design, Simulations, Conclusions, and Future Work Recommendations. The Theory chapter provides the reader with the main knowledge to understand the methods used in the report. The authors however expect the reader to have basic engineering knowledge within mechanics, dynamics and control. The Modelling chapter describes the method of the modelling work. The physics behind the model and how it is used to create a simple state space model of the PT and a more detailed Simulink model of the PT and the vehicle is described. The Control Design chapter describes the method used to design the controllers for the PT model. The chapter also includes a brief summary of the literature covering powertrain controls that has been studied. The Simulations chapter describes the simulations that has been run and how they were carried out. In the Conclusions chapter the main conclusions that has been drawn from the thesis work are stated. Future Work Recommendations is the last chapter, stating some topics that the authors find interesting to look more into.

2 Theory

This chapter intends to describe the theory behind the driveline stabilization issue. Also the theory of how the driveline can be modelled is described as well as the theory behind the control methods applied.

2.1 Driveline Stabilization Issue

The vehicular driveline includes all parts of the powertrain except the prime mover, i.e. the transmission, the shafts and the wheels. As mentioned earlier, the driveline of an electrical vehicle suffers from mechanical resonance as it includes elastic components such as the driveshafts.

2.2 Mechanics and Dynamics

To analyse the driveline, basic mechanical relations as Newton's second law of rotational motion are used. This law implies that for a rigid body the sum of the moment, ΣT , around a fixed rotational point equals to the inertia, J , multiplied with the rotational acceleration, $\dot{\omega}$

$$J\dot{\omega} = \Sigma T \quad (1)$$

The same law for translational motion is

$$ma = \Sigma F \quad (2)$$

The inertia is changed for the mass, m , the angular acceleration for the translational acceleration, a , and the torque for the force, ΣF , is also used. Springs and dampers are used to represent the flexible behaviour of driveshafts and bushings, where the torque, T , equals to the spring coefficient, k , multiplied with the difference in angular position, $\Delta\theta$, for springs

$$T = k\Delta\theta \quad (3)$$

For dampers the torque, T , equals to the damping coefficient, c , multiplied with the angular speed difference, $\Delta\omega$

$$T = c\Delta\omega \quad (4)$$

As the driveline contains a two-step gearbox, the speed ratio, i , between the two gear wheel rotational speeds, ω_1 and ω_2 , in the transmission is expressed as

$$\omega_1 = i\omega_2 \quad (5)$$

2.3 Vehicle Dynamics

In order to analyse the behaviour of the vehicle as well as the effect of the vehicle dynamics on the driveline, the theory of vehicle dynamics is used. The calculations on vehicle dynamics are all based on the ISO8855 coordinate system, see [6].

Focus is put on the longitudinal dynamics, which is defined as the dynamics affecting the vehicle in the travel direction, defined as the x-axis in the ISO8855 standard.

A vehicle's longitudinal dynamics is affected by the driving force, provided by a prime mover, and the external longitudinal forces which in the literature is called driving resistance. The driving resistance is the force that the prime mover needs to overcome to accelerate the vehicle. The driving resistance consists of:

- Wheel resistance
- Air resistance
- Gradient resistance
- Acceleration resistance

Considering a vehicle moving on an inclined road the longitudinal forces acting on the vehicle can be analysed, with longitudinal tyre force at the front tyres, F_{xf} , longitudinal tyre force at the rear tyres, F_{xr} , longitudinal aerodynamical drag force, F_{air} , force due to rolling resistance at the front tyres, R_{xf} , force due to rolling resistance at the rear tyres, R_{xr} , mass of the vehicle, m_v , gravitational acceleration, g , angle of inclination of the road, α . A force balance along the vehicle's longitudinal axis yields

$$m_v a_v = F_{xf} + F_{xr} - F_{air} - R_{xf} - R_{xr} - mg \sin(\alpha) \quad (6)$$

2.3.1 Longitudinal Tyre Force

The longitudinal tyre forces, F_{xf} and F_{xr} , are friction forces acting on the wheels due to the contact with the ground. They depend on the friction coefficient, μ , between tyre and ground, the slip ratio, s_x , and the normal load on the tyre, G_r . The friction coefficient is different for different road surface conditions, tyres and speed. The normal load yields a reaction force, R , acting on the wheel surface, varying with the angle of inclination of the road according to Figure 1.

$$R = G_R \cos(\alpha) \quad (7)$$

On a level surface $R = G_R$.

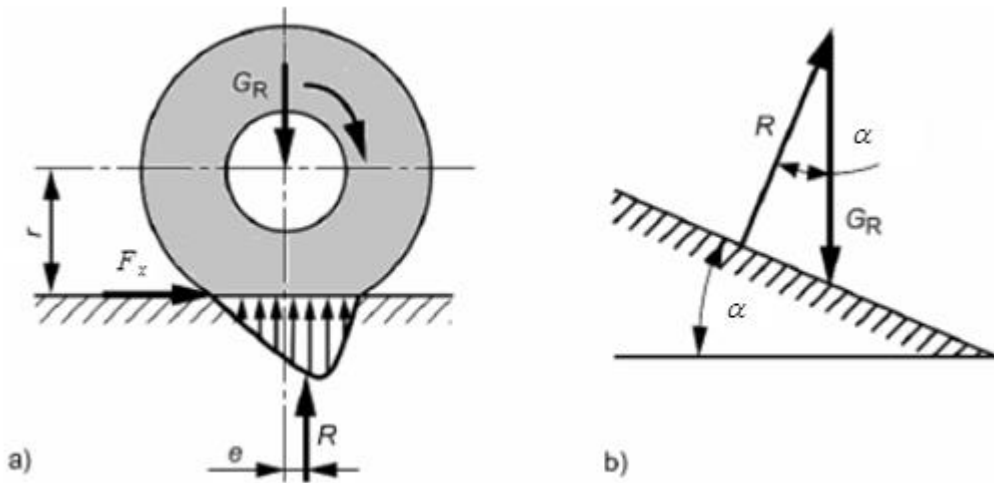


Figure 1. Forces and torque at the wheel. a: On level a road, b: on an inclined road. Figure adapted from [7].

The relation between the reaction force, R , and the longitudinal tyre force F_{xf} or F_{xr} is

$$F_x = \mu R \quad (8)$$

Hence the relation between the normal load, G_r , and the longitudinal tyre force F_{xf} or F_{xr} is

$$F_x = \mu G_R \cos(\alpha) \quad (9)$$

The longitudinal tyre force depends on the tyre slip. In [8] it can be seen that in the case that the slip ratio is small (typically less than 0.1 on dry surface), a linear relation between the longitudinal tyre force, F_x , and the slip ratio, s_x , can be applied as

$$F_x = C_{tyre} s_x \quad (10)$$

where C_{tyre} is the longitudinal tyre stiffness.

A non-linear tyre model, like the Pacejka "Magic Formula" is needed if the slip ratio is not small.

2.3.1.1 Tyre Slip

For a freely rolling wheel the relation between the translational speed, v_v , of the wheel centre and the rotational speed, ω_0 , equals to the effective wheel radius, r_e , as

$$r_e = \frac{v_v}{\omega_0} \quad (11)$$

When a pneumatic tyre is being affected by a driving or braking torque a longitudinal slip arises such that there is a difference between the translational speed and the rotational speed. For a wheel exposed to a driving torque the definition for the longitudinal slip, s_x , according to [9] is

$$s_x = -\frac{v_v - r_e \omega}{v_v} = -\frac{\omega_0 - \omega}{\omega_0} \quad (12)$$

where ω is the actual wheel rotational speed. When a torque is applied, the actual wheel rotational speed, ω , hence is increased compared to the original wheel rotational speed, ω_0 . When a braking torque is applied to the wheel the wheel rotational speed, ω , hence decreases compared to ω_0 . In some literature the equation for the slip is changed to limit the slip to a maximum of one in the case of an applied driving torque. The original rotational wheel speed, ω_0 , in the denominator is then changed for the actual rotational speed, ω , and the equation becomes

$$s_x = -\frac{\omega_0 - \omega}{\omega} = \frac{v_v - \omega r_e}{\omega r_e} = \frac{r_e \omega - v_v}{r_e \omega} \quad (13)$$

which is the equation for tyre slip used in this report.

2.3.1.2 Normal Load

The static normal load on each axle of the vehicle can be determined from the free-body diagram of a static vehicle on an inclined road presented in Figure 2.

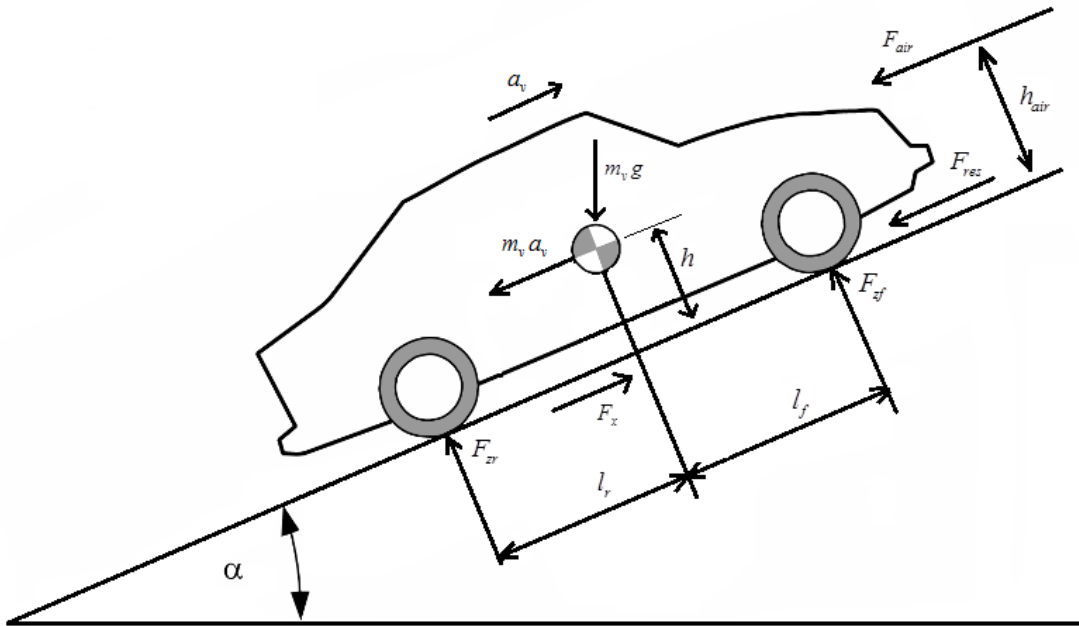


Figure 2. Free Body Diagram for accelerating vehicle. Figure adapted from [7].

Moment equilibrium around the rear contact with ground yields

$$\begin{aligned}
F_{zf}(l_f + l_r) - m_v g(l_r \cos(\alpha) - h \sin(\alpha)) + F_{air} h_{air} &= 0 \Rightarrow \\
\Rightarrow F_{zf} &= m_v g \frac{l_r \cos(\alpha) + h \sin(\alpha)}{l_f + l_r} - F_{air} \frac{h_{air}}{l_f + l_r}
\end{aligned} \tag{14}$$

Moment equilibrium around the front contact with ground yields

$$\begin{aligned}
-F_{zr}(l_f + l_r) + m_v g(l_f \cos(\alpha) + h \sin(\alpha)) + F_{air} h_{air} &= 0 \Rightarrow \\
\Rightarrow F_{zr} &= m_v g \frac{l_f \cos(\alpha) - h \sin(\alpha)}{l_f + l_r} + F_{air} \frac{h_{air}}{l_f + l_r}
\end{aligned} \tag{15}$$

2.3.1.3 Load Transfer Due to Acceleration without Considering Suspension

As the vehicle is accelerating or decelerating, a longitudinal load transfer occurs. This is due to that the CoG creates a torque around the rear contact with the ground or front contact with the ground respectively as the vehicle is being accelerated or decelerated. This can be realized from the free-body diagram in Figure 2 by adding the fictive force caused by the acceleration, $m_v a_v$. Equation (14) and (15) are then modified to equation (16) and (17). Moment equilibrium around the rear contact with the ground gives

$$F_{zf} = m_v g \left(\frac{l_r \cos(\alpha) + h \sin(\alpha)}{l_f + l_r} \right) - m_v a_v \frac{h}{l_f + l_r} - F_{air} \frac{h_{air}}{l_f + l_r} \tag{16}$$

Moment equilibrium around the front contact with the ground gives

$$F_{zr} = m_v g \left(\frac{l_f \cos(\alpha) - h \sin(\alpha)}{l_f + l_r} \right) + m_v a_v \frac{h}{l_f + l_r} + F_{air} \frac{h_{air}}{l_f + l_r} \tag{17}$$

The equations show how the front axle is off-loaded during acceleration meanwhile the rear axle is loaded. The opposite occurs during braking. The equations also show how the air resistance force contributes to off-load the front axle and load the rear axle.

2.3.2 Rolling Resistance

The rolling resistances, R_{xf} and R_{xr} , are modelled as being roughly proportional to the normal forces on each axle, F_{zf} and F_{zr} , as

$$R_{xf} = f F_{zf} \tag{18}$$

and

$$R_{xr} = f F_{zr} \tag{19}$$

where f is the rolling resistance coefficient.

2.3.3 Air Resistance

The air resistance is a quadratic function of the flow rate, v , which is the sum of the vehicle speed and the wind speed. It is calculated from the product of the dynamic pressure, $\frac{1}{2} \rho v^2$, the cross-sectional frontal area of the vehicle, A , and the dimensionless drag coefficient, c_w [7]. Hence the air resistance is represented as

$$F_{air} = \frac{1}{2} \rho c_w A v^2 \quad (20)$$

2.3.4 Gradient Resistance

The gradient resistance is the force due to the gravitation acting on a vehicle travelling up- or downhill and is defined as the component of the total gravitational force in the longitudinal direction of the vehicle. Figure 3 visualizes the gradient resistance of a vehicle.

$$F_g = m_v g \sin(\alpha) \quad (21)$$

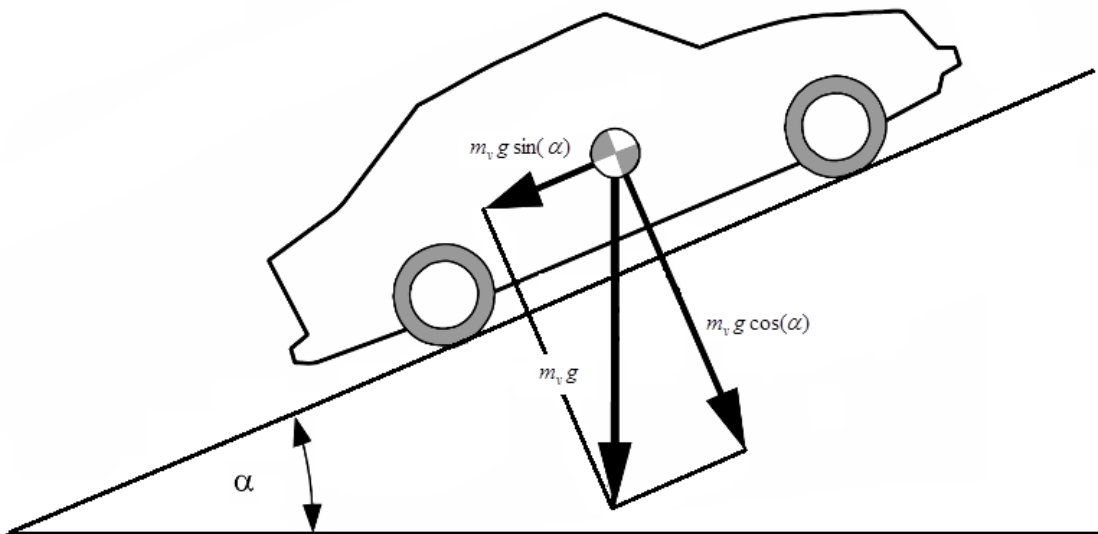


Figure 3. Gradient resistance of a vehicle. Figure adapted from [7].

2.4 Backlash

Backlash is defined as play between adjacent movable parts. It is present in all mechanical systems where a driving member, i.e. the prime mover, is not directly connected to a driven member, i.e. the wheels [10]. E.g. in the gears of a vehicle driveline there is backlash between the teeth in different gear components. Without the backlash the gears would be unable to move. The backlash is a source of problem within the powertrain. It causes issues with driveability. The backlash issues can be noticed during so called *tip-in* and *tip-out* manoeuvres, when the prime mover switches from negative input torque to positive and vice versa.

Initially the gears will be in contact on the negative side of the input gear. When the torque is switched, the contact will cease as the backlash is being traversed. The prime mover will accelerate without the wheels. When all the backlash has been traversed the contact will be recovered, this time on the positive side of the input gear. If the relative speed between the input gear and the output gear is high, a significant part of the momentum built up in the prime mover will be transformed to the wheels and the vehicle will be given a momentary acceleration, called shunt in the literature [11]. The driver will feel the shunt as an uncomfortable jerking of the vehicle. On the other hand, if the backlash is traversed too cautiously the driver will experience a delay between driver command and vehicle acceleration as the backlash is being traversed.

2.4.1 Backlash Modelling

In the MATLAB documentation [12] the backlash block in Simulink is described as a system in which a change in input causes an equal change in output. But when the input changes direction, the output remains unchanged until the backlash has been traversed. The amount of backlash is referred to as the deadband. The deadband is centred about the output. Figure 4 visualises the backlash with a default deadband width of 1 and an initial output of 0.

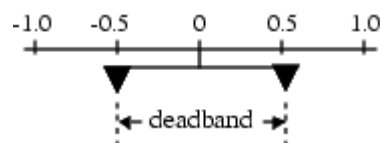


Figure 4. Backlash defined as deadband, with a default width of 1 and an initial output of 0 [12].

The system is non-linear and has three different modes:

1. Non-contact. The input operates in the deadband and the output remains unaffected.
2. Contact in positive direction. The input has reached the positive end of the deadband and engaged the output. The output is equal to the input minus half the deadband width.
3. Contact in negative direction. The input has reached the negative end of the deadband and engaged the output. The output is equal to the input plus half of the deadband width.

Figure 5 visualises the operation of the input in non-contact mode, Figure 6 shows how the input reaches the end of the deadband as the input moves in the positive direction, and hence the system enters the positive contact mode. Figure 7 shows how the output is affected when the input moves in positive direction while the system is in positive contact mode.

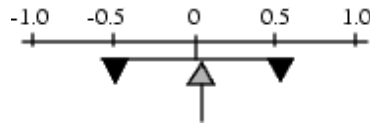


Figure 5. The input operates in the non-contact mode. The output is not affected by the input. [12].

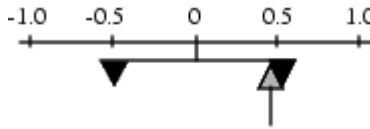


Figure 6. Input reaches the end of the deadband and the positive contact mode is engaged. [12]

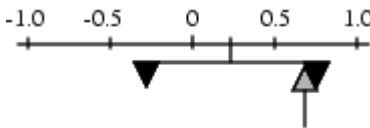


Figure 7. The input moves in positive direction while in positive contact mode. The output equals to the input minus half of the deadband width. [12]

For a vehicle driveline, backlash is present in various parts; in the gearbox, in the differential and in the CV-joints. A frequently used way of modelling backlash is to lump all the different backlashes together and assume that it is connected to a flexible driveshaft. This simplifies the modelling work, one of the reasons why the approach was used in this thesis.

A deadband model of a shaft with backlash is visualized in Figure 8. The deadband width is defined as 2φ and θ_g is the shaft position before the backlash and θ_c is the shaft position after the backlash. The backlash position is defined as $\theta_b = \theta_g - \theta_c$. When $\theta_b < |\alpha|$, the input operates in the deadband zone and the torque on the shaft, T_g , equals to zero. When $\theta_b = -\varphi$, the input is in contact in the negative direction and the torque on the shaft is $T_g < 0$. When $\theta_b = \varphi$, the input is in contact in the positive direction and the torque on the shaft is $T_g > 0$.

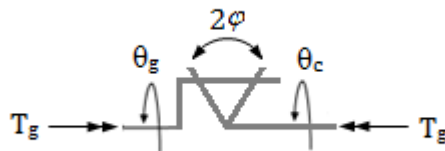


Figure 8. A shaft with backlash.

There are two different principal model structures for backlash mentioned in the literature [11]: Backlash feed-through and backlash feedback. In a backlash feed-through system the dynamics of the output will be affected by the dynamics of the inputs but the reverse will not occur. In the backlash feedback system both sides of the backlash can affect each other. A vehicle powertrain is in need of the latter system since the backlash will be affected by both the dynamics of the prime mover and the dynamics of the vehicle load.

2.5 Wheel Speed Sensor

The wheel speed sensor over the years has become an integral part of the vehicle control systems to improve the performance, efficiency and also safety through systems like antilock braking, electronic stability control, traction control to name a few. In [13] it is mentioned that wheel speed sensors used for automotive purposes are mainly two types: Electromagnetic and digital speed sensors. Electromagnetic speed sensor works on Hall effect principle with two components; a rotating ferrous wheel with teeth/lines, and a fixed sensor whose magnetic field detects the teeth/lines of the wheel and sends out a pulse for each teeth/line. The digital sensor can be either Hall effect sensor or optical sensor, with the newer version being equipped with a filter which extract a square wave from the sinusoidal signal of the sensor.

The sensors placed at the wheels come with disadvantages as well. In [14] it is mentioned that they have to be placed very close to the ferrous metal teeth to produce adequate output voltage. They are susceptible to noise and bad resolution at low speeds with near zero speeds being almost impossible to sense. For these reasons wheel speed sensor signals are usually further filtered (signal processing techniques) or use a model based estimation as mentioned in [13]. Figure 9 shows how a wheel speed signal from a sensor compares to that of actual wheel speed.

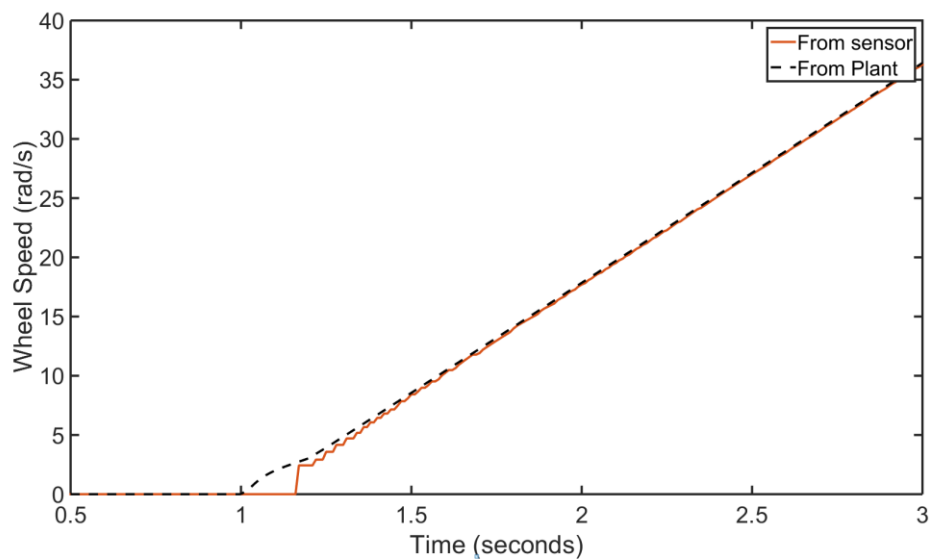


Figure 9. Wheel speed Actual vs. from sensor.

2.6 LQR

[15] describes Linear Quadratic Regulator as an optimal control strategy that can be successfully implemented for tackling vibration suppression problems in linear vibrating systems. There are two approaches in LQR: State LQR optimal problem, State-output LQR optimal problem.

Consider a linear time-invariant system, both controllable and observable

$$\begin{aligned}\dot{x} &= Ax + Bu \\ y &= Cx\end{aligned}\tag{22}$$

with initial state conditions

$$x(0) = x_0\tag{23}$$

where, $x = [x_1, x_2, x_3 \dots x_n]^T$ is a state vector, $u = [u_1, u_2, u_3 \dots u_m]^T$ is an inputs/controls vector, $y = [y_1, y_2, y_3 \dots y_n]^T$ is a column vector of output with matrices A and B having the following dimensions $\dim A = n \times n$, $\dim B = n \times m$, $\dim C = r \times n$.

2.6.1 State LQR Optimal Problem:

The state control law tries to minimize the cost function

$$J = \frac{1}{2} \int_0^{\infty} (x^T Q_{LQR} x + u^T R_{LQR} u) dt\tag{24}$$

subject to differential equation (22) and initial conditions (23). The matrices Q_{LQR} a positive definite matrix and R_{LQR} a positive definite matrix are real coefficient symmetric weighting matrices which can be tuned the controller by penalizing the states accordingly. This results in a controller of the form

$$u_{*LQR} = -G_{LQR} x\tag{25}$$

where G_{LQR} is the gain matrix which on multiplying with the state vector provides an optimum feedback to stabilize the system. The gain matrix can be calculated as

$$G_{LQR} = R_{LQR}^{-1} B^T S_{LQR}\tag{26}$$

where S_{LQR} is a positive definite matrix and the unique solution of the Riccati matrix equation given by

$$A^T S_{LQR} + S_{LQR} A - S_{LQR} B R_{LQR}^{-1} B^T S_{LQR} + Q_{LQR} = 0\tag{27}$$

This will result in an optimal system state determined by the solution to the initial value problem

$$\dot{x} = [A - B R_{LQR}^{-1} B^T S_{LQR}] x \quad x(0) = x_0\tag{28}$$

2.6.2 State-output LQR (LQRY) Optimal Problem:

The state output control law tries to minimize the cost function

$$J = \frac{1}{2} \int_0^{\infty} (y^T Q_{LQRY} y + u^T R_{LQRY} u) dt \quad (29)$$

subject to the differential equation (22) and initial conditions (23). The matrices Q_{LQRY} , an $r \times r$ positive definite matrix, and R_{LQRY} , an $m \times m$ positive definite matrix, are real coefficient symmetric weighting matrices which can be tuned by penalizing the states accordingly. This results in a controller of the form

$$u_{*LQRY} = -G_{LQR} x \quad (30)$$

where G_{LQR} is the gain matrix which on multiplying with the state vector provides an optimum feedback, u_* , to stabilize the system. The gain matrix can be calculated as

$$G_{LQR} = R_{LQRY}^{-1} B^T S_{LQRY} \quad (31)$$

where S_{LQRY} is a positive definite matrix and unique solution of the Riccati matrix differential equation given by

$$A^T S_{LQRY} + S_{LQRY} A - S_{LQRY} B R_{LQRY}^{-1} B^T S_{LQRY} + C^T Q_{LQRY} C = 0 \quad (32)$$

This will result in an optimal system state determined by the solution to the initial value problem

$$\dot{x} = [A - B R_{LQRY}^{-1} B^T S_{LQRY}] x \quad x(0) = x_0 \quad (33)$$

2.7 LQ Estimator

In [1] and [16] a description of using an estimator is presented, which will result in a control feedback of the form

$$u_{*E} = -G_E \hat{x} \quad (34)$$

where \hat{x} is the vector of state estimates. Assume the following plant with process noise w and measurement noise v

$$\begin{aligned} \dot{x} &= Ax + Bu + w \\ y &= Cx + v \end{aligned} \quad (35)$$

If the covariances for the noises are written as

$$E(w w^T) = W \quad E(v v^T) = V \quad E(w v^T) = N \quad (36)$$

the estimator gain K derived will be of the form

$$K = PC^T V^{-1} \quad (37)$$

where P is the solution to the Riccati equation

$$AP + PA^T - (PC^T + N)V^{-1}(CP + N^T) + W = 0 \quad (38)$$

The equation for the resultant observer is of the form

$$\dot{\hat{x}} = A\hat{x} + Bu + K(y - C\hat{x}) \quad (39)$$

The plant, controller and observer can be represented as shown in Figure 10.

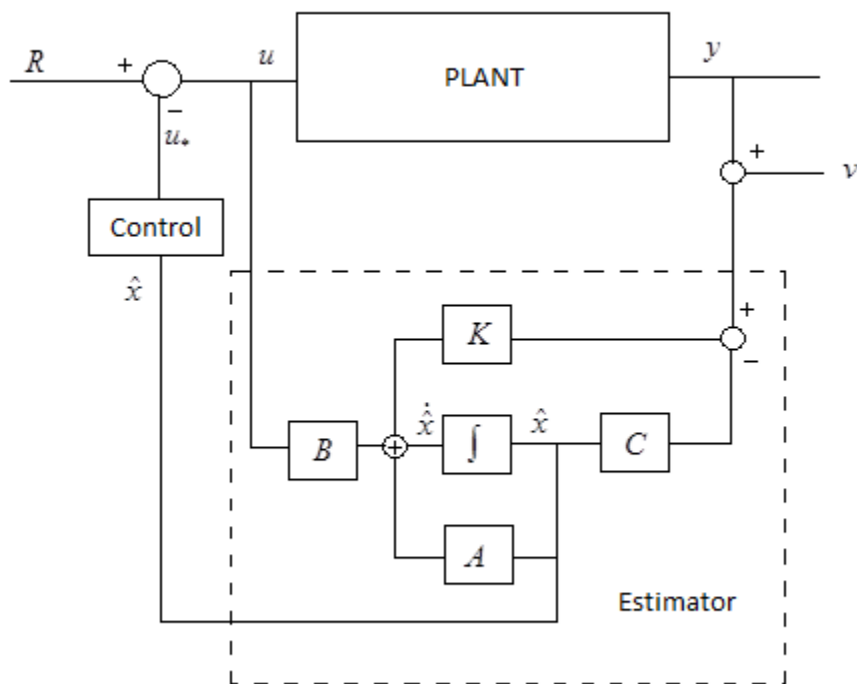


Figure 10. Layout of plant, controller and estimator.

3 Modelling

This chapter describes the physics behind the model and how it is used to set up a simple state space model of the powertrain. The last part of the chapter describes how the more advanced Simulink model was built up.

3.1 Making of the Powertrain and Vehicle Model

The approach when modelling the powertrain and vehicle is to develop two models in parallel; a simple model that could be expressed in state space form, and a more advanced model built up in Simulink. The reason for this is that the controller chosen required a model in state space form to calculate the controller gain while a more advanced model is required to make an analysis of e.g. the driveline backlash and wheel slip possible. More about this in section 3.3.

Since one of the purposes of building the model is to create a controller for the EM based on the model it is of great importance that the model captures the main characteristics of the driveline. The oscillations in the driveline are the most important of these characteristics. In [17] it has been shown that a simplified third order powertrain model where the masses are lumped and linked together by torsional, linear and massless springs and dampers is sufficient to capture the characteristics. Such a third order model is visualized in Figure 11.

No differential is used in either the state space model or the Simulink model, which means that a single driveshaft and wheel is representing the two driveshafts and wheels in the vehicle. This implies that the values used for driveshaft stiffness, driveshaft damping and tyre longitudinal stiffness throughout the report equals to twice the corresponding values in the vehicle.

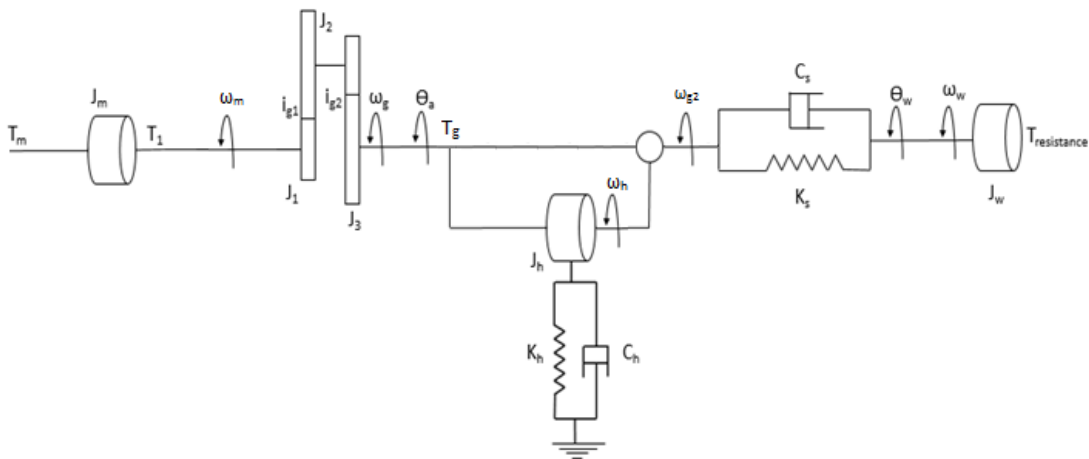


Figure 11. Powertrain model with lumped inertias for electric motor, gearbox, powertrain housing and wheel.

3.1.1 Electric Motor

The first lumped mass in the powertrain model presented in Figure 11 corresponds to the rotating part of the electric motor, EM. Its dynamics are described by equation (1), Newton's second law of rotational motion.

$$J_m \dot{\omega}_m = T_m - T_1 \quad (40)$$

where J_m is the motor inertia, $\dot{\omega}_m$ is the motor rotational acceleration, T_m is the input torque before the rotational inertia of the EM and T_1 is the output torque after the rotational inertia of the EM.

3.1.2 Gearbox

The gearbox, GB, is of two-stage single speed type, transforming the speed in two steps. Figure 12 is a magnification of the GB in Figure 11. The GB is considered to have three lumped inertias; J_1 represents the rotational inertia for the input shaft and its gear wheel, J_2 the intermediate shaft and its two gear wheels and J_3 the output shaft and its gear wheel.

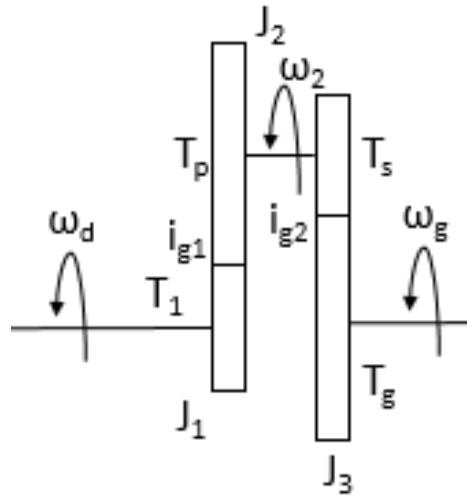


Figure 12. Two stage single-speed gearbox with three lumped inertias.

The primary gear step transforms the motor's outgoing speed as per equation (5)

$$\omega_2 = \frac{\omega_m}{i_{g1}} \quad (41)$$

The secondary gear step transforms the outgoing speed from the primary gear step as

$$\omega_g = \frac{\omega_2}{i_{g2}} \quad (42)$$

The resulting total GB gear ratio hence is

$$i = i_{g1} i_{g2} \quad (43)$$

and the total speed transformation from the motor's outgoing shaft to the GB's outgoing shaft is described as

$$\omega_g = \frac{\omega_m}{i} \quad (44)$$

Newton's second law of rotational motion describes the relation between the lumped rotational inertia of the input shaft, J_1 , its rotational acceleration, $\dot{\omega}_m$, which is the same as for the EM, the input torque, T_1 , and the output torque, T_p

$$J_1 \dot{\omega}_m = T_1 - T_p \quad (45)$$

The same holds for the second gear step, using the lumped rotational inertia of the intermediate shaft, J_2 , its rotational acceleration, $\dot{\omega}_2$, the input torque, which is obtained by multiplying the input shaft torque with the primary gear ratio, i_{g1} , and the output torque, T_s

$$J_2 \dot{\omega}_2 = (i_{g1} T_p) - T_s \quad (46)$$

The same relation is also applied to the third lumped mass, obtaining the input torque by multiplying the output torque from intermediate shaft with the secondary gear ratio, i_{g2}

$$J_3 \dot{\omega}_g = (i_{g2} T_s) - T_g \quad (47)$$

It is desired to express the input torque on the input shaft of the GB in relation to the output torque on the output shaft of the GB, excluding the input and output torque on the intermediate shaft. Equation (47) can be rewritten as

$$T_s = \frac{J_3 \dot{\omega}_g}{i_{g2}} + \frac{T_g}{i_{g2}} \quad (48)$$

Equation (46) can be rewritten as

$$T_p = \frac{J_2 \dot{\omega}_2}{i_{g1}} + \frac{T_s}{i_{g1}} \quad (49)$$

Equation (45) can be rewritten as

$$T_1 = J_1 \dot{\omega}_m + T_p \quad (50)$$

Inserting equation (48) into equation (49) and then equation (49) into equation (50) while substituting $\dot{\omega}_2$ with $\dot{\omega}_m$ using equation (41) and $\dot{\omega}_g$ with $\dot{\omega}_m$ using equation (42) yields

$$T_1 = J_1 \dot{\omega}_m + \frac{J_2 \dot{\omega}_m}{i_{g1}^2} + \frac{J_3 \dot{\omega}_m}{(i_{g1} i_{g2})^2} + \frac{T_g}{i_{g1} i_{g2}} \quad (51)$$

By inserting equation (51) into equation (40) the inertias of the EM and GB are lumped together and an expression for the dynamics from the EM's input shaft to the GB's output shaft follows

$$J_m \dot{\omega}_m = T_m - \left(J_1 \dot{\omega}_m + \frac{J_2 \dot{\omega}_m}{i_{g1}^2} + \frac{J_3 \dot{\omega}_m}{(i_{g1} i_{g2})^2} + \frac{T_g}{i_{g1} i_{g2}} \right) \Leftrightarrow$$

$$\dot{\omega}_m \left(J_m + J_1 + \frac{J_2}{i_{g1}^2} + \frac{J_3}{(i_{g1} i_{g2})^2} \right) = T_m - \frac{T_g}{i_{g1} i_{g2}} \quad (52)$$

3.1.3 Powertrain Housing

The non-rotating parts of the EM and GB are stiffly mounted together and hereafter called PT housing. The PT housing is mounted to the vehicle chassis using four rubber bushings. The rubber bushings are flexible and can, as the driveshafts, be described as a spring and damper in parallel using equation (3) and (4). The representation of the bushings is simplified to a single spring in parallel with a single damper. The stiffness is k_h and the damping coefficient is c_h . The vehicle chassis is considered stiff, why the angular position and speed of the chassis is defined as zero. The mass of the powertrain housing is lumped and its rotational inertia is J_h . The housing can be considered mounted parallel with the output shaft of the GB, as can be seen in Figure 13, which is a magnification of the PT housing part of the model presented in Figure 11.

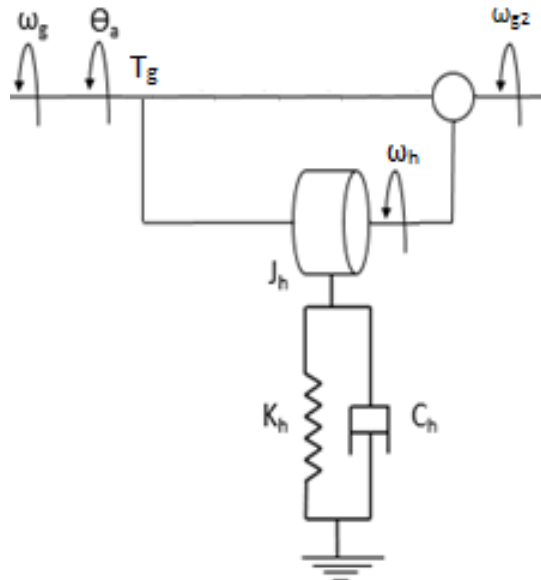


Figure 13. Powertrain housing with powertrain mountings.

The torque that is put into the PT housing is the torque on the output shaft of the GB, T_g . The rotational acceleration of the lumped PT housing inertia, $\dot{\omega}_h$, is expressed with equation (1)

$$J_h \dot{\omega}_h = T_g - k_h \theta_h - c_h \omega_h \Leftrightarrow \dot{\omega}_h = \frac{T_g}{J_h} - \frac{k_h \theta_h}{J_h} - \frac{c_h \omega_h}{J_h} \quad (53)$$

The effective rotational acceleration that the driveshaft experiences, $\dot{\omega}_{g,eff}$, with respect to the vehicle chassis, will be the difference between the rotational acceleration of the output shaft of the gearbox, $\dot{\omega}_g$, and the rotational acceleration of the PT housing, $\dot{\omega}_h$

$$\dot{\omega}_{g,eff} = \dot{\omega}_g - \dot{\omega}_h \quad (54)$$

The PT housing is not modelled in the simple model, however it is modelled in the Simulink model.

3.1.4 Driveshaft

The driveshaft can be described as a damped torsional flexibility [16] and thus modelled as a spring and damper in parallel using equation (3) and (4). The torque in the driveshaft is the sum of the torque in the spring and the damper, where k_s is the driveshaft stiffness, c_s is the driveshaft damping coefficient, $\theta_{g,eff}$ is the angular position at the end of the driveshaft connected with the gearbox, θ_w is the angular position at the end of the driveshaft connected with the wheel, $\omega_{g,eff}$ and ω_w are the corresponding rotational speeds. The torque due to damping is small in comparison to the torque due to stiffness since the damping coefficient is small compared to the stiffness coefficient. The driveshaft torque can be written as

$$T_g = k_s (\theta_{g,eff} - \theta_w) + c_s (\omega_{g,eff} - \omega_w) \quad (55)$$

Not considering the PT housing, the driveshaft torque can be expressed as

$$T_g = k_s (\theta_g - \theta_w) + c_s (\omega_g - \omega_w) \quad (56)$$

As mentioned in the beginning of the chapter the driveshaft stiffness and damping coefficient equals to twice the corresponding values of the vehicle since the model uses a single driveshaft.

3.1.5 Wheel

The last lumped mass of the model corresponds to the wheel. The wheel experiences a torque from the driveshaft, T_g , and a counteracting traction torque, T_{trac} . Equation (1) is used to describe the dynamics of the wheel

$$J_w \dot{\omega}_w = T_g - T_{trac} \quad (57)$$

The traction torque is the effective torque put into the ground by the wheel. It can be transformed to a traction force as

$$T_{trac} = F_{trac} r \quad (58)$$

The traction force is counteracted by a resistance force, F_{res} , which derives from all the forces acting on the vehicle body and that needs to be overcome to accelerate the vehicle mass, m_v , with a certain acceleration, a_v . Equation (2) is used to describe this relation.

$$m_v a_v = F_{trac} - F_{res} \quad (59)$$

The resistance force is summed up by the wheel resistance, F_w , the aerodynamical resistance, F_{air} , and the gradient resistance, F_{grad} . See section 2.3 for a more thorough presentation. Equation (58) and equation (59) are inserted into equation (57) to express the wheel dynamics in terms of resistance torque and acceleration.

$$J_w \dot{\omega}_w = T_g - (m_v a_v + F_{res}) r \quad (60)$$

For the simple state space model the wheel is assumed to roll without slip, which implies that the vehicle speed, v_v , can be expressed as the product of the wheel radius, r , and the rotational wheel speed, ω_w

$$v_v = r \omega_w \quad (61)$$

The assumption of no wheel slip also implies that the vehicle acceleration, a_v , can be expressed as

$$a_v = r \dot{\omega}_w \quad (62)$$

Inserting equation (62) into equation (60) yields

$$J_w \dot{\omega}_w + m_v r^2 \dot{\omega}_w = T_g - T_{res} \quad (63)$$

Exchanging the driveshaft torque, T_g , using equation (56) and rewriting the equation results in the following expression for the wheel acceleration

$$\dot{\omega}_w = \frac{k_s (\theta_g - \theta_w) + c_s (\omega_g - \omega_w) - T_{res}}{J_w + m_v r^2} \quad (64)$$

3.2 State Space Model

Three state variables are introduced; the torsion in the driveshaft, the motor speed and the wheel speed. The PT housing is not considered for the state space model, why the torsion in the driveshaft can be expressed as

$$\begin{aligned}x_1 &= \theta_g - \theta_w \\x_2 &= \omega_m \\x_3 &= \omega_w\end{aligned}\tag{65}$$

The EM acceleration is derived by inserting equation (51) into equation (40)

$$\begin{aligned}\dot{\omega}_m &= \frac{T_m}{J_m} - \frac{1}{J_m} \left(J_1 \dot{\omega}_m + \frac{J_2 \dot{\omega}_m}{i_{g1}^2} + \frac{J_3 \dot{\omega}_m}{(i_{g1} i_{g2})^2} + \frac{T_g}{i_{g1} i_{g2}} \right) \Leftrightarrow \\ \dot{\omega}_m &= \frac{T_m}{J_m} - \dot{\omega}_m \left(\frac{J_1}{J_m} + \frac{J_2}{J_m i_{g1}^2} + \frac{J_3}{J_m (i_{g1} i_{g2})^2} \right) - \frac{T_g}{J_m i_{g1} i_{g2}} \Leftrightarrow \\ \dot{\omega}_m + \dot{\omega}_m \left(\frac{J_1}{J_m} + \frac{J_2}{J_m i_{g1}^2} + \frac{J_3}{J_m (i_{g1} i_{g2})^2} \right) &= \frac{T_m}{J_m} - \frac{T_g}{J_m i_{g1} i_{g2}} \\ \dot{\omega}_m \left(1 + \frac{J_1}{J_m} + \frac{J_2}{J_m i_{g1}^2} + \frac{J_3}{J_m (i_{g1} i_{g2})^2} \right) &= \frac{T_m}{J_m} - \frac{T_g}{J_m i_{g1} i_{g2}}\end{aligned}\tag{66}$$

Introducing J_e to simplify equation (66)

$$J_e = 1 + \frac{J_1}{J_m} + \frac{J_2}{J_m i_{g1}^2} + \frac{J_3}{J_m (i_{g1} i_{g2})^2}\tag{67}$$

the EM acceleration can be expressed as

$$\dot{\omega}_m = \frac{T_m}{J_e J_m} - \frac{T_g}{J_e J_m i_{g1} i_{g2}}\tag{68}$$

Inserting the expression for the driveshaft torque from equation (56) yields

$$\dot{\omega}_m = \frac{T_m}{J_e J_m} - \frac{k_s (\theta_g - \theta_w) + c_s (\omega_g - \omega_w)}{J_e J_m i_{g1} i_{g2}}\tag{69}$$

Inserting equation (43) into equation (69) gives an expression for the EM speed that is expressible with the other states

$$\dot{\omega}_m = \frac{T_m}{J_e J_m} - \frac{k_s(\theta_g - \theta_w) + c_s(\frac{\omega_m}{i} - \omega_w)}{J_e J_m i_{g1} i_{g2}} \Leftrightarrow \quad (70)$$

$$\dot{\omega}_m = -\frac{k_s \theta_g}{J_e J_m i_{g1} i_{g2}} + \frac{k_s \theta_w}{J_e J_m i_{g1} i_{g2}} - \frac{c_s \omega_m}{J_e J_m (i_{g1} i_{g2})^2} + \frac{c_s \omega_w}{J_e J_m i_{g1} i_{g2}} + \frac{T_m}{J_e J_m}$$

No resistance torque, T_{res} , is considered for the state space model. By setting $T_{res} = 0$, introducing a lumped inertia, J_v , for the vehicle

$$J_v = J_w + m_v r^2 \quad (71)$$

and inserting equation (44) and equation (71) into equation (64), the wheel acceleration can be expressed as

$$\dot{\omega}_w = \frac{k_s(\theta_g - \theta_w) + c_s(\frac{\omega_m}{i} - \omega_w)}{J_v} \Leftrightarrow \quad (72)$$

$$\dot{\omega}_w = \frac{k_s \theta_g}{J_v} - \frac{k_s \theta_w}{J_v} + \frac{c_s \omega_m}{J_v i} - \frac{c_s \omega_w}{J_v}$$

The derivative of the three state variables (65) can now be written as

$$\dot{x}_1 = \frac{\omega_m}{i_{g1} i_{g2}} - \omega_w \Leftrightarrow \dot{x}_1 = \frac{x_2}{i_{g1} i_{g2}} - x_3$$

$$\dot{x}_2 = -\frac{k_s \theta_g}{J_e J_m i_{g1} i_{g2}} + \frac{k_s \theta_w}{J_e J_m i_{g1} i_{g2}} - \frac{c_s \omega_m}{J_e J_m (i_{g1} i_{g2})^2} + \frac{c_s \omega_w}{J_e J_m i_{g1} i_{g2}} + \frac{T_m}{J_e J_m} \Leftrightarrow \quad (73)$$

$$\dot{x}_2 = -\frac{k_s x_1}{J_e J_m i_{g1} i_{g2}} - \frac{c_s x_2}{J_e J_m (i_{g1} i_{g2})^2} + \frac{c_s x_3}{J_e J_m i_{g1} i_{g2}} + \frac{T_m}{J_e J_m}$$

$$\dot{x}_3 = \frac{k_s \theta_g}{J_v} - \frac{k_s \theta_w}{J_v} + \frac{c_s \omega_m}{J_v i_{g1} i_{g2}} - \frac{c_s \omega_w}{J_v} \Leftrightarrow \dot{x}_3 = \frac{k_s x_1}{J_v} + \frac{c_s x_2}{J_v i_{g1} i_{g2}} - \frac{c_s x_3}{J_v}$$

The powertrain model can now be written in state space form. Equation (43) for the total GB gear ratio is inserted

$$\vec{\dot{x}} = \begin{bmatrix} 0 & \frac{1}{i} & -1 \\ -\frac{k_s}{J_e J_m i} & -\frac{c_s}{J_e J_m i^2} & \frac{c_s}{J_e J_m i} \\ \frac{k_s}{J_v} & \frac{c_s}{J_v i} & -\frac{c_s}{J_v} \end{bmatrix} \vec{x} + \begin{bmatrix} 0 \\ 1 \\ 0 \end{bmatrix} T_m = \mathbf{A}\vec{x} + \mathbf{B}\vec{u} \quad (74)$$

3.3 Simulink Model

The Simulink model (See Appendix II: Simulink Model) was built up in blocks representing the different parts; the EM and GB, the PT housing, the driveshaft, the wheel, the tire and the vehicle body. The powertrain and vehicle model is, as the state space model, simplified using a single driveshaft, a single wheel and a single tyre. Hence no differential has been used.

3.3.1 Electric Motor and Gearbox

In the Simulink model the EM and GB inertias are lumped together in a single block and the total GB gear ratio, i , from equation (43) is used to calculate the EM rotational acceleration, $\dot{\omega}_m$, according to equation (52). The inputs of the block are the torque on the EM input shaft, T_m , and the torque on the GB output shaft, T_g . The EM rotational acceleration is integrated to achieve the EM rotational speed, ω_m , which is divided with the total GB gear ratio, i , to achieve the GB output shaft rotational speed, ω_g . In turn, the GB output shaft rotational speed is integrated, which yields the GB output shaft position, θ_g . The latter two are the outputs of the EM and GB block.

3.3.2 Power Saturation

The EM has a maximum torque limit and also a maximum power limit. To replicate the EM power characteristics in the simulations it is necessary to make sure that the EM never delivers torque or power above these limits. The curve in Figure 14 represents the limits of the EM. The torque limits the curve at lower speed while the power limits the curve at higher speed, which explains the shape of the curve. A look-up table generated from the curve in Figure 14 was used to saturate the input torque. The look-up table is placed within the EM and GB block and reads the actual EM speed and puts out a maximum allowable torque, which is fed back and compared with the demanded input torque. The smallest torque is chosen and sent as input to the EM.

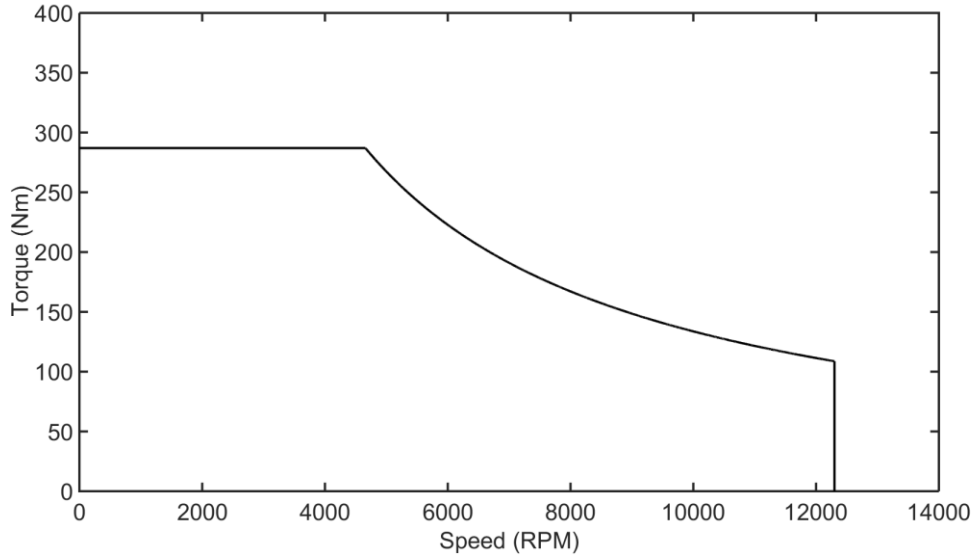


Figure 14. EM torque versus speed plot representing the limited torque and power of the machine.

3.3.3 PT Housing

The driveshaft torque, T_g , is the only input into the PT housing block. The block outputs the PT housing position, θ_h . It is calculated through integrating the PT housing rotational acceleration, $\dot{\omega}_h$, twice, which is calculated with equation (53), subtracting the torque due to stiffness and damping in the PT housing bushings from the driveshaft torque. The PT housing position, θ_h , is subtracted from the GB output shaft position, θ_g , in a separate block succeeding the PT housing to achieve the effective driveshaft position, $\theta_{g,eff}$, according to equation (54).

3.3.4 Backlash

All the driveline backlash is lumped together and put in a block in between the PT housing and the driveshaft. The Simulink block used to generate the backlash is called backlash and is explained in greater detail in section 2.4. The backlash is added to the effective driveshaft position, $\theta_{g,eff}$. A new effective driveshaft position will yield from this, $\theta_{g,eff,b}$. The new effective driveshaft position is derived to achieve the corresponding driveshaft rotational speed, $\omega_{g,eff,b}$. The effective position and speed are the outputs of the backlash block.

The backlash will operate as a *backlash feedback system*, since it is connected to the driveshaft and therefore is in a closed-loop system as the output shaft torque, T_g , is fed back into the EM and GB block, as well as the PT housing block, to generate the effective driveshaft position, $\theta_{g,eff}$.

3.3.5 Driveshaft

The driveshaft block has the angular position at the end of the driveshaft connected to the GB, i.e. the effective driveshaft position after adding backlash,

$\theta_{g,eff,b}$, as well as the angular position at the end of the driveshaft connected to the front wheel, θ_{wf} , as inputs. The corresponding rotational speeds, $\omega_{g,eff,b}$ and ω_{wf} , are also put into the block.

The shaft torsion is now calculated as the difference between the effective GB side driveshaft end position, $\theta_{g,eff,b}$, and the wheel side driveshaft end position, θ_{wf} . The speed difference between the driveshaft ends is also calculated, subtracting the front wheel speed, ω_{wf} , from the GB side driveshaft end speed, $\omega_{g,eff,b}$. The torque due to stiffness and damping, which is the driveshaft torque, T_g , is now calculated according to equation (55). The driveshaft torque is the only output from the driveshaft block.

3.3.6 Wheel

The wheel block contains two parallel models, one for the rear wheels which are not affected by a driving torque, and one for the front wheels, which are driven. The inputs into the wheel block are the driveshaft torque, T_g , the effective longitudinal tyre force for the front wheels, $F_{xf,eff}$, and for the rear wheels, $F_{xr,eff}$. The effective longitudinal tyre force is the difference between the available longitudinal traction force and the resisting longitudinal force at the tyre. See section 2.3.1 and section 3.1.5 for a more thorough explanation. For the front wheels the effective longitudinal tyre force, $F_{xf,eff}$, is multiplied with the wheel radius, r , to achieve the corresponding torque, then subtracted from the driveshaft torque, T_g , and divided with the wheel inertia, J_w , to obtain the wheel rotational acceleration. Note that the effective tyre torque is used instead of the traction as in equation (57), since the wheel rolling resistances, R_{xf} and R_{xr} , are already subtracted from the tyre traction forces, F_{xf} and F_{xr} , in the tyre block. The rear wheels will only experience the effective longitudinal tyre force since they are not driven. Hence the rear rotational wheel acceleration is calculated by dividing the effective longitudinal tyre force, $F_{xf,eff}$, with the wheel inertia, J_w . The rotational wheel accelerations are integrated to obtain the rotational wheel speeds, ω_{wf} and ω_{wr} , which are the outputs of the wheel block together with the front wheel angular position, θ_{wf} , which is obtained by integrating the front wheel speed, ω_{wf} , again. The front wheel angular position is fed back to the driveshaft block.

3.3.7 Tyre

The tyre block, like the wheel block, also has two parallel models for the front and the rear wheels respectively. The inputs are the rotational wheel speeds, ω_{wf} and ω_{wr} , the vehicle translational speed, v_v , the normal load for the front axle, F_{zf} , and the normal load for the rear axle, F_{zr} . The rolling resistances, R_{xf} and R_{xr} , are calculated with equation (18) and (19), where the normal forces, F_{zf} and F_{zr} , are

calculated with equation (7), to consider the effect of an inclined road. The rolling resistances are then multiplied with the sign of the wheel speed to make the rolling resistances valid for negative wheel speeds as well.

The longitudinal tyre forces, also called the traction forces, F_{xf} and F_{xr} , are calculated as the slip ratio, s_x , multiplied with the longitudinal tyre stiffness, C_{tyre} , according to equation (10). The slip ratio is calculated according to equation (13), where the rotational wheel speed, ω , is multiplied with the effective wheel radius, r_e , the vehicle translational speed, v_v , is subtracted and the sum divided by the product of the rotational wheel speed, ω , and the effective wheel radius, r_e . A MinMax block was used for the product in the denominator, where the greater input was chosen between a constant equal to one and the mentioned product. The approach was chosen to omit the problem of dividing with zero when starting the simulation with a wheel speed of zero.

The effective longitudinal tyre forces, $F_{xf,eff}$ and $F_{xr,eff}$, are calculated as the difference between the traction forces, F_{xf} and F_{xr} , and the rolling resistance forces, R_{xf} and R_{xr} , respectively, as per equation (59). The outputs from the tyre block are the effective longitudinal tyre forces, $F_{xf,eff}$ and $F_{xr,eff}$, and the rolling resistances, R_{xf} and R_{xr} .

3.3.8 Vehicle Body

The inputs into the vehicle body block are the effective longitudinal tyre forces, $F_{xf,eff}$ and $F_{xr,eff}$, and the rolling resistances, R_{xf} and R_{xr} . The remaining “driving resistances”; the air resistance and the gradient resistance are calculated in a common block inside the vehicle body block. Its input is the vehicle speed, v_v , and its output is the sum of the air resistance, F_{air} , and the gradient resistance, F_g . The air resistance is calculated as a product of the air density, ρ , the vehicle’s frontal area, A , the drag coefficient, c_w , and the square of the vehicle speed, v_v . The square of the vehicle speed is multiplied with the sign of the vehicle speed to make the air resistance valid for negative speeds. The product is divided with a factor two, according to equation (20). The gradient resistance, F_g , is calculated as the product of the vehicle’s mass, m_v , the gravitational acceleration, g , and sine of the gradient as per equation (21).

The air resistance and the gradient resistance are subtracted from the effective longitudinal tyre forces, $F_{xf,eff}$ and $F_{xr,eff}$, resulting in the effective translational force on the vehicle, which is divided by the vehicle mass, m_v , to obtain the vehicle acceleration, a_v , according to equation (6). The vehicle acceleration is then integrated to obtain the vehicle speed, v_v , which is fed back into the air- and gradient resistance block.

The load transfer is calculated in a block inside the vehicle body block. Its input is the vehicle acceleration, a_v , and its outputs are the normal loads on the front axle, F_{zf} , and the rear axle, F_{zr} . The normal loads are calculated according to equation (16) and (17) respectively. A product block for each term in the numerator was created. In the first block for the front axle load, F_{zf} , the vehicle mass, m_v , is multiplied with the gravitational acceleration, g , the distance between the rear axle and the CoG, l_r , and cosine of the gradient, $\cos(\alpha)$. The same product is used for the rear axle load, F_{zr} , replacing the the distance between the rear axle and the CoG with the distance between the front axle and the CoG, l_f . The next term is calculated as the vehicle mass, m_v , multiplied with the gravitational acceleration, g , the distance from the ground to the CoG, h , and sine of the gradient, $\sin(\alpha)$. The next term is calculated as the vehicle mass, m_v , multiplied with the vehicle acceleration, a_v , and the distance from the ground to the CoG, h . The last term is calculated as the air resistance force, F_{air} , multiplied with the distance from the ground to the CoP, h_{air} . The terms are summed up according to equation (16) and (17) respectively and then divided with the wheel base, which is the sum of the distance between the rear axle and the CoG, and the distance between the front axle and the CoG, $l_f + l_r$.

The outputs from the vehicle body block are the normal loads on each axle, F_{zf} and F_{zr} , the vehicle speed, v_v , and the total vehicle resistance.

4 Control Design

This chapter describes the method used to design the controllers for the driveline. First, a brief summary of applicable control methods found in the literature are described.

In [2], a study was conducted on different approaches like using filters as compensators, virtual inertia of rotor, virtual damping factor of the half shafts for damping the oscillations were assessed for their functionality and performance. The conclusion produced in [2] is that using pure filters is very inflexible and are not recommended as good solutions, and the same goes in case of using pure virtual inertia where the electromagnetic torque to be produced had to be at a frequency higher than the first natural frequency of the mechanical driveline which is not a good idea due to limiting factors like bandwidth of traction drives etc. It concluded that implementing a virtual driveshaft damping using active control algorithm would be the best solution and is extremely robust and stable. In [1], different linear control strategies like PID, pole placement and Linear Quadratic controller are looked into. The Linear Quadratic control was concluded to be the most effective solution among others. [4], [5], [3] and [18] investigate in

using special filters, cascade based control, and special control structures to damp the resonance frequency and actively damp the oscillations in the driveline which can be possible solutions as well. According to the work in, [1], [19] and [20] control techniques based on Linear Quadratic design have been used, and in [19] the controller was extended to incorporate backlash handling which showed promising results. On discussing about the usable data it was considered that using the motor speed and wheel speeds from the sensors would be the most feasible option for inputs to the state observer.

4.1 Virtual Physical Damper

By the Virtual Physical Damper approach a gain value equivalent to a damping factor is used to produce a feedback torque value which is a resultant from the product of gain value and speed difference between the two ends of the driveshaft. This feedback torque is intended to reduce the speed difference thus damping the shaft oscillations. The reference damper in theory will be imitating a damper that is connected in parallel to the driveshaft. The reference damper model will be used to benchmark another active control damping strategy for effectiveness and performance verification. The layout of model with virtual physical damper is shown in Figure 15.

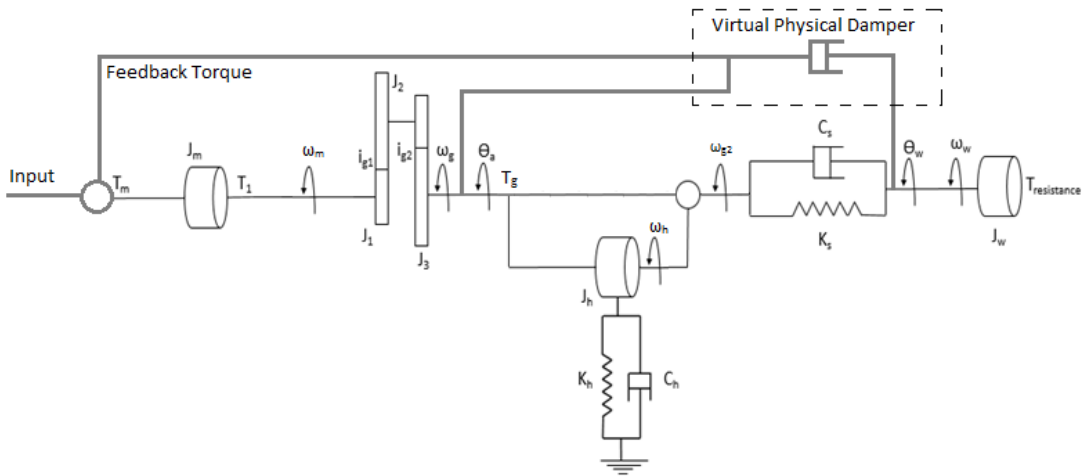


Figure 15. Virtual physical damper structure.

4.2 LQ Estimator

As mentioned in the theory about the problems with the wheel speed data which can lead to erratic behaviour of the controllers estimating the wheel speed seemed to be a good way to tackle the issue by using the motor speed as estimator reference since EM speed data received is of high resolution and good quality. The covariance matrices, W and V , are tuned accordingly. The matrix W is tuned to represent the weighting for estimator process values, matrix V is tuned to represent the weighting for sensor (motor speed from modelled plant) values.

4.3 LQR

By using a linear model and the availability of all the states from the estimator, LQR is a good option to go with. The LQR controller developed was based on using the shaft torsion which is the first state in the state vector, i.e. using the Q_{LQR} matrix, the shaft torsion was penalized for damping out the oscillations. The Q_{LQR} matrix was kept diagonal for ease of penalizing interpretation, a positive large entry was made for the diagonal element in Q_{LQR} that will relate to the shaft torsion state and the other diagonal elements were kept to the minimum. The R_{LQR} matrix was a 1×1 with value tuned to control the feedback torque value thus defining the controller to be aggressive or not. The elements in the weighting matrices representing the states being controlled and feedback control signal are divided by the square of the assumed peak (or the range of operation) that we expect the controller to limit to. This is done so that the values are normalized thus ensuring no misinterpretation of the penalized terms by the controller during the reduction of the cost function. To calculate the control gain for the system in MATLAB a direct command “lqr” is used. The structure of the method is the same as that of the LQRY which is represented in Figure 16.

4.4 LQRY

The LQRY is an extension of the LQR method. It works by output weighting. This provides more flexibility in controlling the system based on the output matrix design, thus not having to rely solely on the states of the model. LQRY was chosen to use with rate of shaft torsion (which can also be explained as speed difference at the shaft ends) as weighting output which will try to minimize the difference between the frequency of oscillations at the shaft ends thus not effecting the phase difference (which is the effective torsion in the shaft equivalent to the torque experienced at the shaft). This will also help in reducing the size of Q_{LQRY} matrix down to the components of interest. Tuning of the weighting matrices are also done in the same way as that of LQR. To calculate the control gain for the system in MATLAB a direct command “lqry” is used.

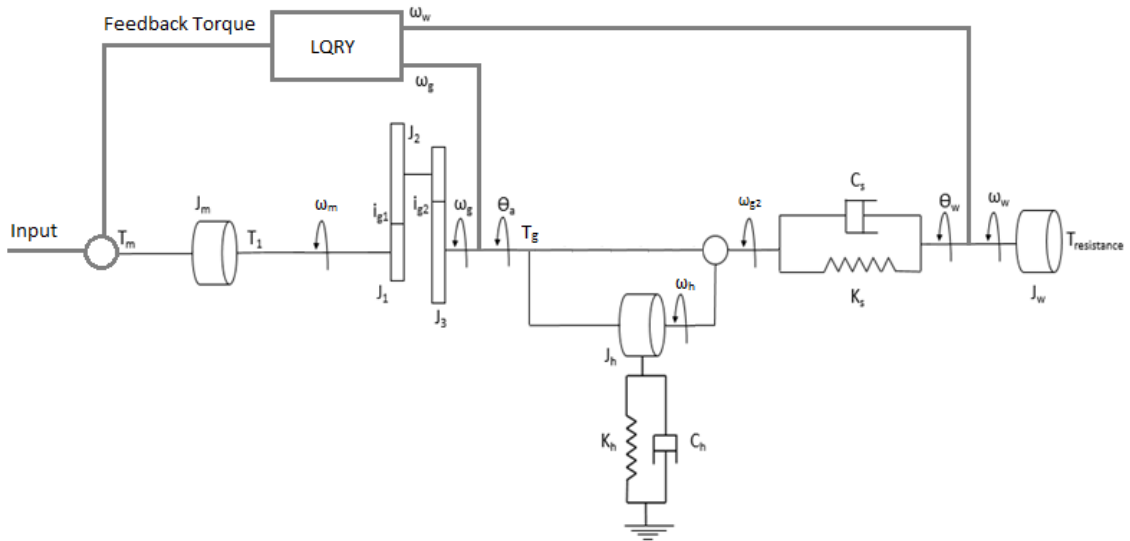


Figure 16. LQRY structure.

4.5 Controller Torque Saturation

In the same way as the input torque of the EM is saturated by the torque and power limits of the EM in section 3.3.2, it is necessary to make sure that the controller does not request for more torque than which the system is able to provide. To ensure that the controller torque is limited within the allowable values a *torque saturation control* was added after the damping controller. The controller contains the same look-up table as in section 3.3.2, which in this block reads the estimated EM speed and puts out an allowable torque value. This allowable torque value is compared with the effective torque from the damping controller. If the allowable torque is more than the effective torque from the damping controller then no change is made to the torque from the damping controller, but on the other hand if the effective torque from damping controller is more than the allowable torque, the power saturation control limits the effective torque down to the allowable torque.

4.6 Backlash Estimation

Estimating backlash and using that state to include in the controller is one kind of approach. In this process the controller and the estimator are linearized at two operating points namely *contact mode* and *non-contact mode*. In contact mode it is assumed that the backlash region has been traversed and there is a torque transfer along the system. In non-contact mode it is assumed that the system is traversing through the backlash region and that there is no complete torque transfer in the system. A new state space is developed based on the preliminary state space model with an added state for backlash estimation and control.

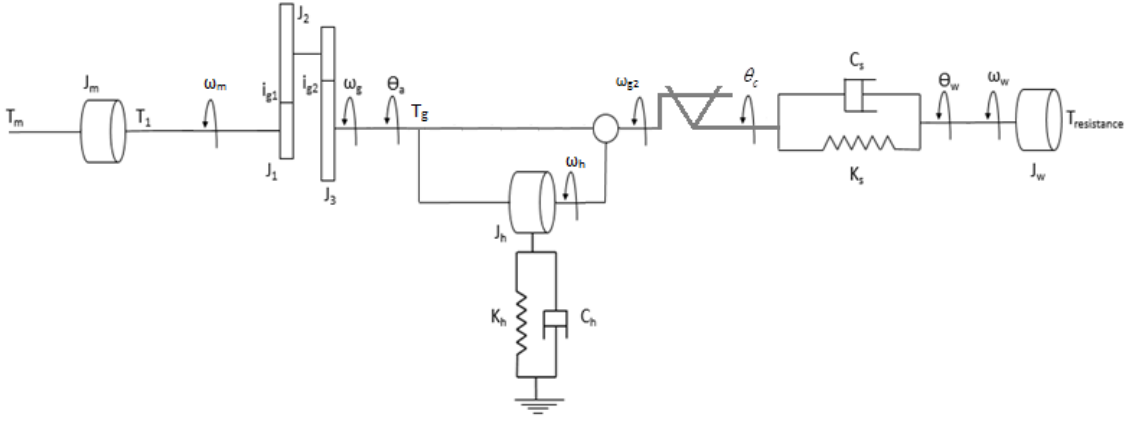


Figure 17. Plant with backlash.

By looking at the plant model in Figure 17 and neglecting the housing for the state space generation, the following can be stated for the two operating points:

4.6.1 Contact Mode

The angular position, θ_g , is switched for θ_c in equation (70) and (72), according to Figure 17, leading to

$$\dot{\omega}_m = \frac{T_m}{J_e J_m} - \frac{K_s}{J_e J_m i} (\theta_c - \theta_w) - \frac{C_s}{J_e J_m i} (\dot{\theta}_c - \omega_w) \quad (75)$$

$$\dot{\omega}_w = \frac{K_s}{J_w + (mr^2)} (\theta_c - \theta_w) + \frac{C_s}{J_w + (mr^2)} (\dot{\theta}_c - \omega_w) - \frac{T_l}{J_w + (mr^2)} \quad (76)$$

If $\theta_b = \theta_g - \theta_c$ is the backlash position and $\theta_g = \frac{\theta_m}{i}$, equation (75) and (76) can be rewritten as

$$\dot{\omega}_m = \frac{T_m}{J_e J_m} - \frac{K_s}{J_e J_m i} \left(\frac{\theta_m}{i} - \theta_b - \theta_w \right) - \frac{C_s}{J_e J_m i} \left(\frac{\omega_m}{i} - \dot{\theta}_b - \omega_w \right) \quad (77)$$

$$\dot{\omega}_w = \frac{K_s}{J_w + (mr^2)} \left(\frac{\theta_m}{i} - \theta_b - \theta_w \right) + \frac{C_s}{J_w + (mr^2)} \left(\frac{\omega_m}{i} - \dot{\theta}_b - \omega_w \right) - \frac{T_l}{J_w + (mr^2)} \quad (78)$$

In case of contact mode $\omega_b = 0$, as there will not be any change in the backlash position.

The state space model can be written as

$$\begin{bmatrix} \dot{\omega}_m \\ \dot{\omega}_w \\ \dot{\theta}_m \\ \dot{\theta}_w \\ \dot{T}_l \\ \dot{\omega}_b \end{bmatrix} = \begin{bmatrix} 0 & 0 & 1 & 0 & 0 & 0 \\ 0 & 0 & 0 & 1 & 0 & 0 \\ \frac{-K_s}{J_m J_e i^2} & \frac{K_s}{J_m J_e i} & \frac{-C_s}{J_m J_e i^2} & \frac{C_s}{J_m J_e i} & 0 & \frac{K_s}{J_m J_e i} \\ \frac{K_s}{(J_w + mr^2)i} & \frac{-K_s}{J_w + mr^2} & \frac{C_s}{(J_w + mr^2)i} & \frac{-C_s}{J_w + mr^2} & -1 & \frac{-K_s}{J_w + mr^2} \\ 0 & 0 & 0 & 0 & 0 & 0 \\ 0 & 0 & 0 & 0 & 0 & 0 \end{bmatrix} \begin{bmatrix} \theta_m \\ \theta_w \\ \omega_m \\ \omega_w \\ T_l \\ \theta_b \end{bmatrix} + \begin{bmatrix} 0 \\ 0 \\ 1 \\ 0 \\ 0 \\ 0 \end{bmatrix} \frac{T_m}{J_m J_e} \quad [79]$$

4.6.2 Non-contact Mode

In case of no contact between the components, meaning that the backlash region is being traversed, there should be effectively no torque transfer through the driveshaft, so the torque on the driveshaft is considered to be zero. The resultant equations will be in the form

$$T_s = K_s \left(\frac{\theta_m}{i} - \theta_b - \theta_w \right) + C_s (\omega_m - \omega_b - \omega_w) = 0 \quad (80)$$

$$\omega_b = -\omega_w + \frac{\omega_m}{i} + \frac{K_s}{C_s} \left(\frac{\theta_m}{i} - \theta_b - \theta_w \right) \quad (81)$$

$$\dot{\omega}_m = \frac{T_m}{J_e J_m} \quad (82)$$

$$\dot{\omega}_w = \frac{-T_l}{J_w + mr^2} \quad (83)$$

The state space equation for this linearized point changes to

$$\begin{bmatrix} \dot{\omega}_m \\ \dot{\omega}_w \\ \dot{\omega}_m \\ \dot{\omega}_w \\ \dot{T}_l \\ \dot{\omega}_b \end{bmatrix} = \begin{bmatrix} 0 & 0 & 1 & 0 & 0 & 0 \\ 0 & 0 & 0 & 1 & 0 & 0 \\ 0 & 0 & 0 & 0 & 0 & 0 \\ 0 & 0 & 0 & 0 & \frac{-1}{J_w + mr^2} & 0 \\ 0 & 0 & 0 & 0 & 0 & 0 \\ \frac{K_s}{C_s i} & \frac{-K_s}{C_s} & \frac{1}{i} & -1 & 0 & \frac{-K_s}{C_s} \end{bmatrix} \begin{bmatrix} \theta_m \\ \theta_w \\ \omega_m \\ \omega_w \\ T_l \\ \theta_b \end{bmatrix} + \begin{bmatrix} 0 \\ 0 \\ 1 \\ 0 \\ 0 \\ 0 \end{bmatrix} T_m \quad [84]$$

4.7 Backlash Controller

To traverse the backlash region so that the controller's performance is not effected, a separate control strategy is implemented at the end along the chain of control. This controller does not allow for quick transients of the input torque until the backlash region is completely traversed. It does so by referencing to the estimated shaft torsion and ramping up the effective control torque by a tuned slope value until the estimated shaft torsion reaches a set value and later hands over the system to the active damping control to damp out the oscillations. In this way the non-linearity is overcome beforehand to prevent the controllers from destabilizing.

This method was chosen as an alternate from using the estimated backlash values due to certain issues that occur with estimation which are discussed further in section 5.19.

5 Simulations

This chapter includes the method, results and discussion of the simulations carried out within the thesis.

5.1 Frequency Response Plots for State Space Model

The powertrain model in state space form described in section 3.2 was analysed in the frequency domain, plotting the Bode diagrams for the transfer function from EM torque, T_m , to wheel speed, ω_w , to visualize the shuffle phenomena. Figure 18 shows the phase and magnitude for the transfer function. From the diagram it can be seen that the powertrain model has a resonance peak at 81.4 rad/s, which equals to 12.95 Hz.

Due to the presence of powertrain housing mounts in close interaction with the driveshafts, if we consider for an effective stiffness, assuming the mounts and driveshaft stiffness to be in series

$$Effective\ stiffness = \frac{K_h K_s}{K_h + K_s} \approx 11150\ Nm/rad \quad (85)$$

$$Effective\ resonance\ frequency = \sqrt{\frac{Effective\ stiffness}{\frac{J_m J_e i^2}{2\pi}}} \approx 8.55\ Hz \quad (86)$$

This is the resonance peak that implies the shuffle phenomena of the vehicle. The resonance peak is within the frequency range 0 to 40 Hz, which is the range influencing the driveability. Thus it can be perceived by the driver.

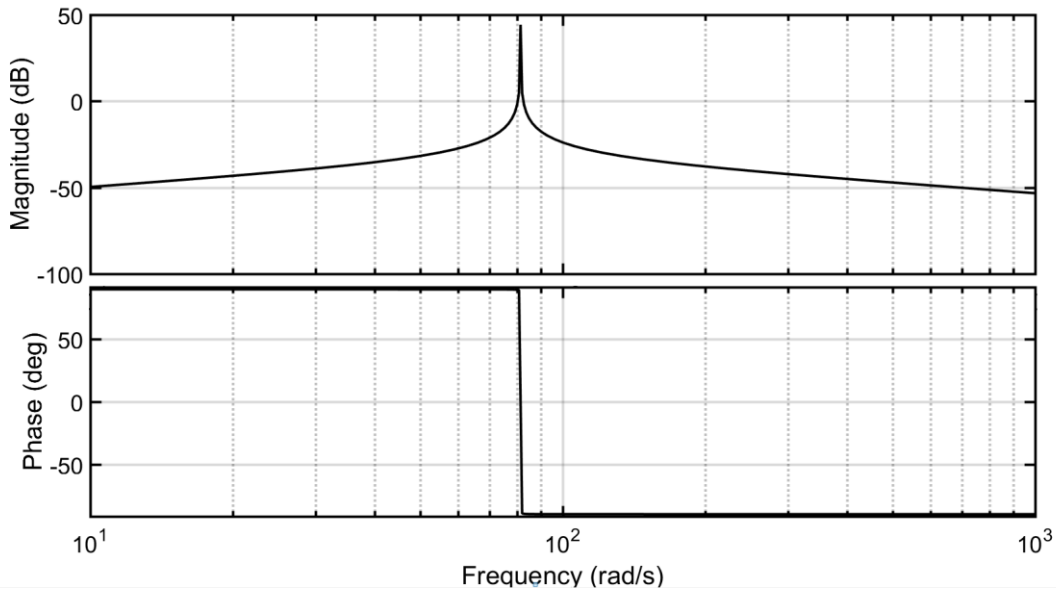


Figure 18. The Bode diagrams for the transfer function from motor torque to wheel speed for the state space model of the powertrain.

5.2 Plant Model

The powertrain model created in Simulink and described in section 3.3 is a model of the powertrain without any damping other than the small damping in the driveshaft, for a step input of the maximum available motor torque of 287 Nm, the shuffle phenomena is clearly visible. In Figure 19 it can be noticed as torque oscillations in the driveshaft. The oscillations are significant with an initial amplitude of over 4200 Nm, before they get dampened out. However, a step input of the maximum EM torque, where the maximum torque is reached instantaneously is an aggressive case. In reality the torque would rather be ramped up. Also, the real powertrain includes more damping than the model, i.e. viscous damping in the gearbox and differential and damping in form of losses as gear meshing losses. Hence the oscillations in the model are probably more extensive than in the real powertrain.

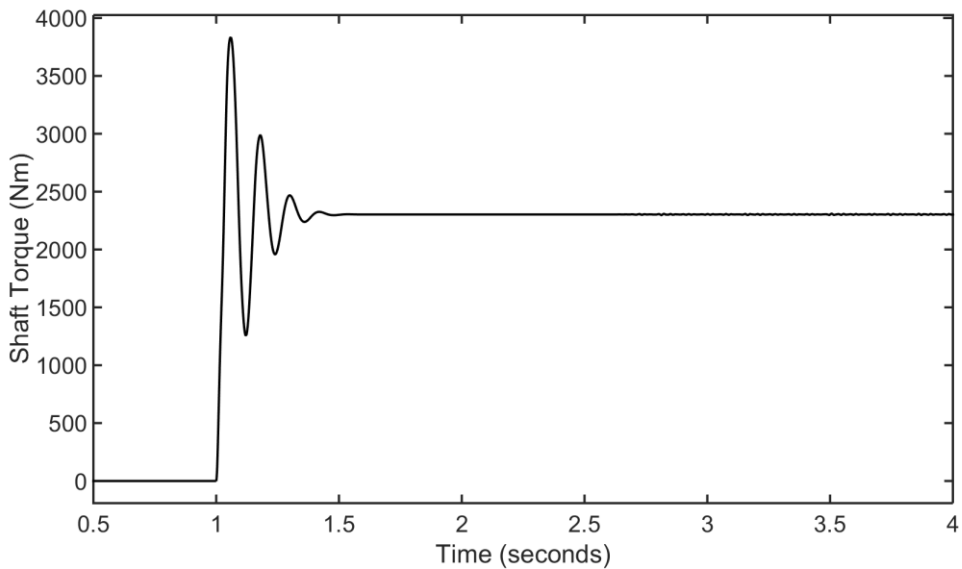


Figure 19. Shaft torque for a step input of 287 Nm for the powertrain model.

The torque oscillations in the driveshaft transforms directly to vehicle acceleration oscillations, that can be seen in Figure 20. The shuffle phenomena results in a "jerking" effect of the vehicle, which is easier to relate to as a driveability issue.

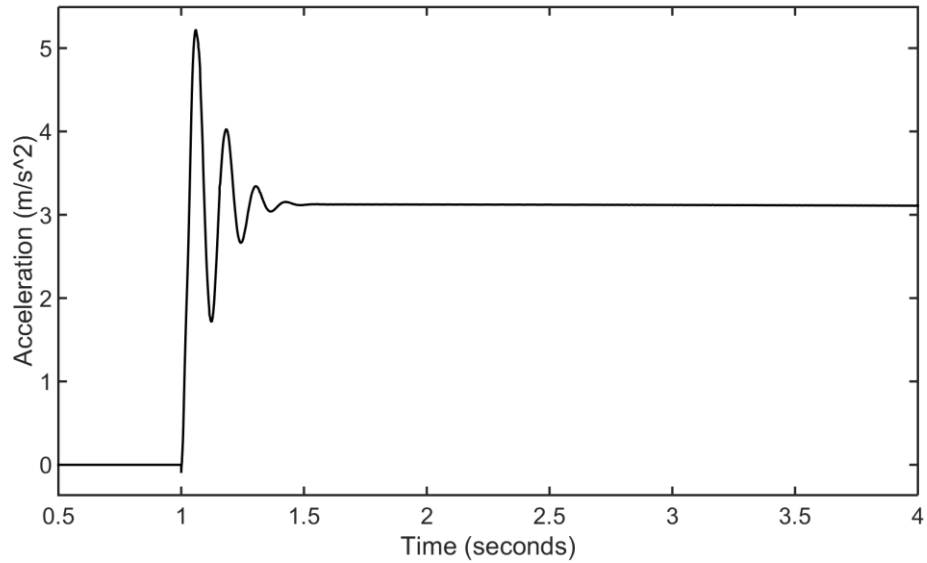


Figure 20. Vehicle acceleration for a step input of 287 Nm for the powertrain model.

5.3 Powertrain Model with Virtual Physical Damper

When the powertrain model was equipped with a virtual physical damper, feeding the EM with an additional torque to dampen out the oscillations observed in Figure 19, and giving the same step input of 287 Nm, the torque response in the driveshaft shows no tendencies of oscillations, as can be seen in Figure 22. The damping coefficient was tuned until the best trade-off between fast response and effective damping was found. If the damping coefficient is too low there will still be torque oscillations initially. If the damping coefficient is too high the time to reach peak torque will increase, i.e. the response time will increase. In turn it will result in the vehicle accelerating slower. It was found that a damping coefficient of 72 Nms/rad gave good results. Figure 21 visualizes how the input signal to the motor is modified when the virtual physical damper controller using states directly from the plant is implemented.

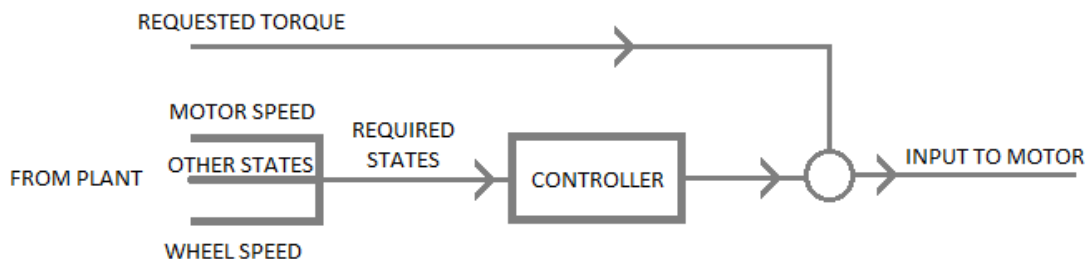


Figure 21. Only controllers with states from plant directly.

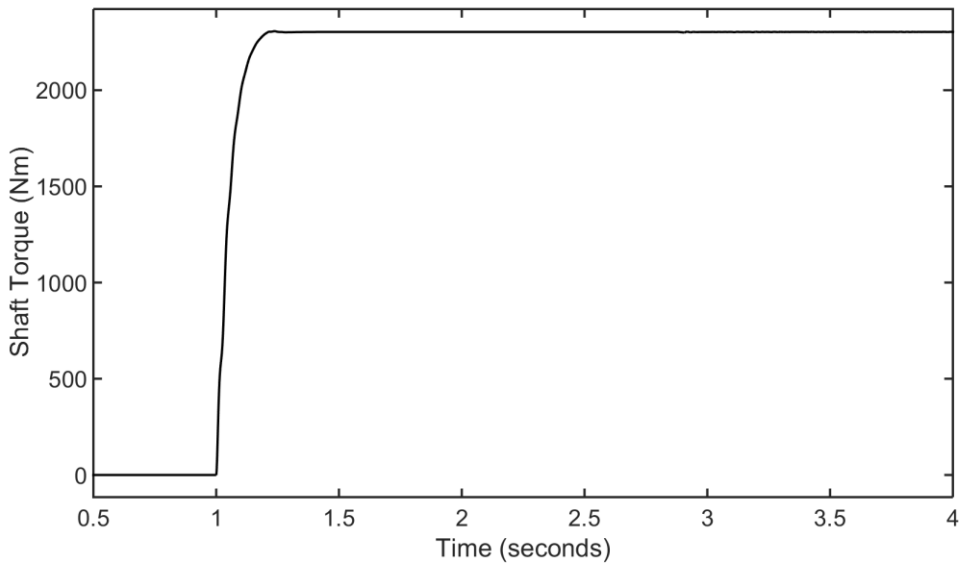


Figure 22. Shaft torque for a step input of 287 Nm for the powertrain model with a feedback torque generated by a virtual physical damper.

Figure 23 shows three graphs with different tuned damping coefficients for the damper. The solid line corresponds to a damping coefficient of 72 Nms/rad, the dashed line corresponds to 110 Nms/rad and the dotted line corresponds to 30 Nms/rad. It is clearly visible how the lower damping coefficient results in initial oscillations, as well as the higher damping coefficient results in an increased response time.

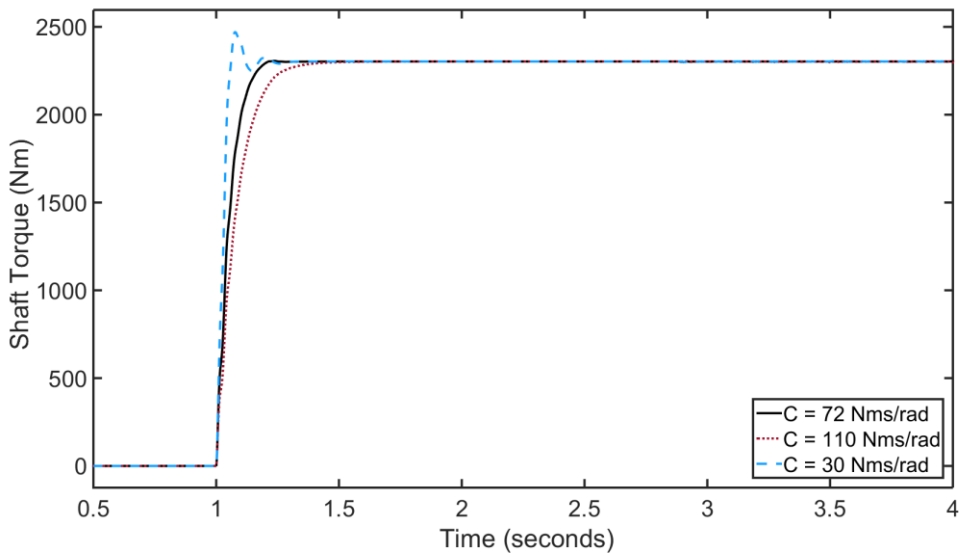


Figure 23. Shaft torque for a step input of 287 Nm for the powertrain model with a feedback torque generated by a virtual, physical damper. The solid line corresponds to the model with a damper with damping coefficient, c , of 80 Nms/rad, the dashed line corresponds to a model with damping coefficient of 120 Nms/rad and the dotted line corresponds to a model with damping coefficient of 40 Nms/rad.

The results from controlling the motor torque by feeding back the torque measured by the physical damper are impressive. The oscillations are dampened out effectively.

5.4 Virtual Physical Damper Using Wheel Speed Sensor

For the plots made until here the signals needed for the controller has been taken directly from the real, actual signals in the powertrain model. However, when running the controller in a vehicle, the signal from the wheel speed sensor is not as good as the signal from the Simulink model, as is explained in section 2.5. The signal is time-discrete and also time-delayed. A model for a time-discrete and delayed wheel speed sensor was added to the powertrain model and the signal was used instead of the optimal signal from the model itself. The motor speed signal however has a good resolution compared to the wheel speed signal. An assumption was therefore made that the signal from the powertrain model could still be used. Figure 24 visualizes the input signal to the motor when the virtual physical damper controller using a wheel speed signal from a sensor is implemented.

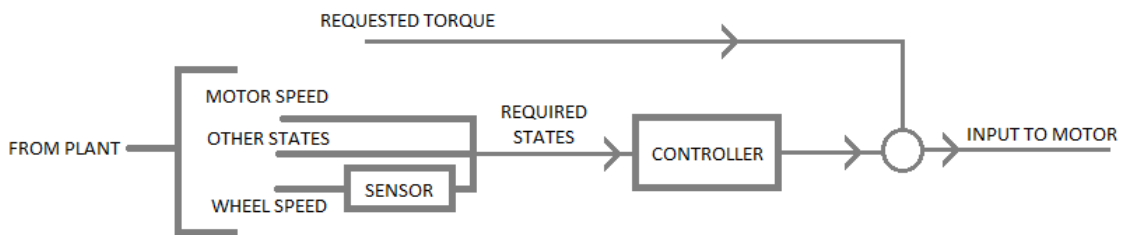


Figure 24. Wheel speed sensor implementation.

Figure 25 shows the response torque in the driveshaft for a step input of 287 Nm for the powertrain model using the virtual physical damper as controller and a wheel speed signal provided by the model of the wheel speed sensor described above. The model seems to behave strangely, the driveshaft torque shows some oscillations that were not seen in the powertrain model using the optimal signal for the wheel speed. The strange behaviour is explained by the issues that come with the wheel speed sensor, such as being time-delayed and having a low resolution.

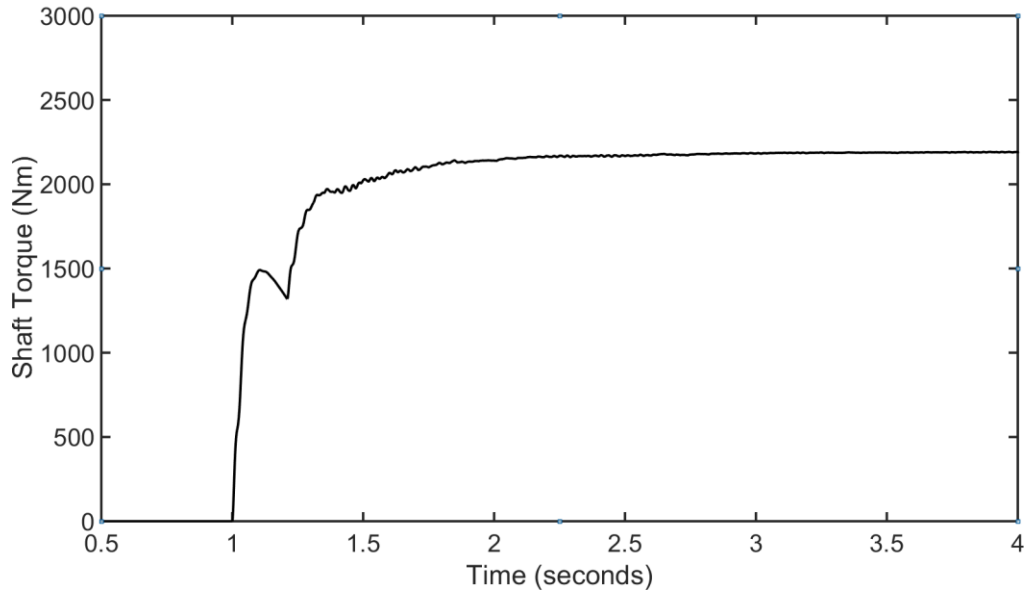


Figure 25. Shaft torque for a step input of 287 Nm for the powertrain model with a feedback torque generated by the physical damper and a wheel speed signal provided by a wheel speed sensor model.

5.5 Checking for Possibility of Improvement in Physical Damper by Varying Controller Damping Value.

As it can be seen from Figure 25 the wheel speed signal with lower resolution is leading to reduced performance and increased response time, simulations were performed with different damping values for the physical damper to evaluate the possibility of improving its performance by tuning the damping value. Four damping values 60, 72, 100, 120 (all values have the unit Nms/rad) were used for this evaluation. The results can be seen in Figure 26.

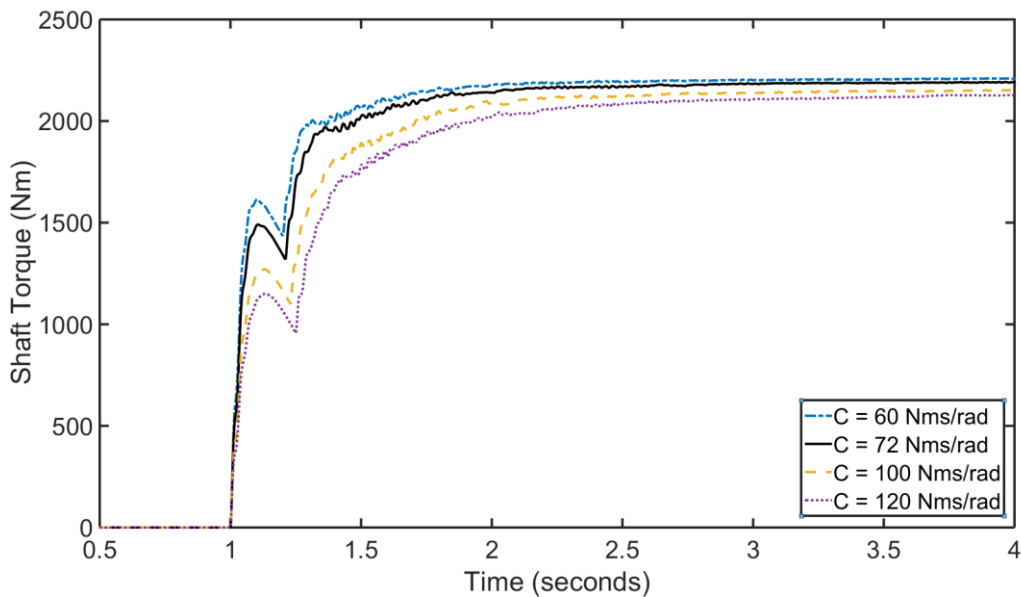


Figure 26. Physical damper with wheel speed sensor for different damping values.

By changing the damping values it can be observed that there is no significant improvement in terms of performance as the driveshaft oscillations are not

completely damped out in the beginning, i.e. during the rise period of the driveshaft torque.

5.6 Implementing Estimator

To improve the virtual physical damper performance, an estimator described in section 4.2, was added so that better values of the wheel speed could be used to improve the controller performance. Figure 27 visualizes the input signal to the motor when the virtual physical damper controller using a wheel speed signal from an estimator is implemented.

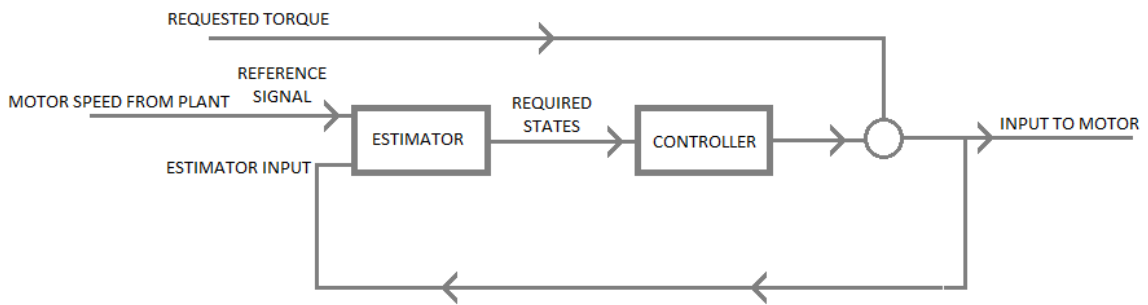


Figure 27. Estimator with one reference signal implemented.

A simulation was run for a requested step torque of 287 Nm. It can be seen from the shaft torque plot in Figure 28 that using estimated state values is aiding in mitigating the ill effects of using wheel speed from the sensor directly for the states required by the controller. But to achieve this the damping value had to be retuned and a value of 125 Nms/rad showed to be giving good values.

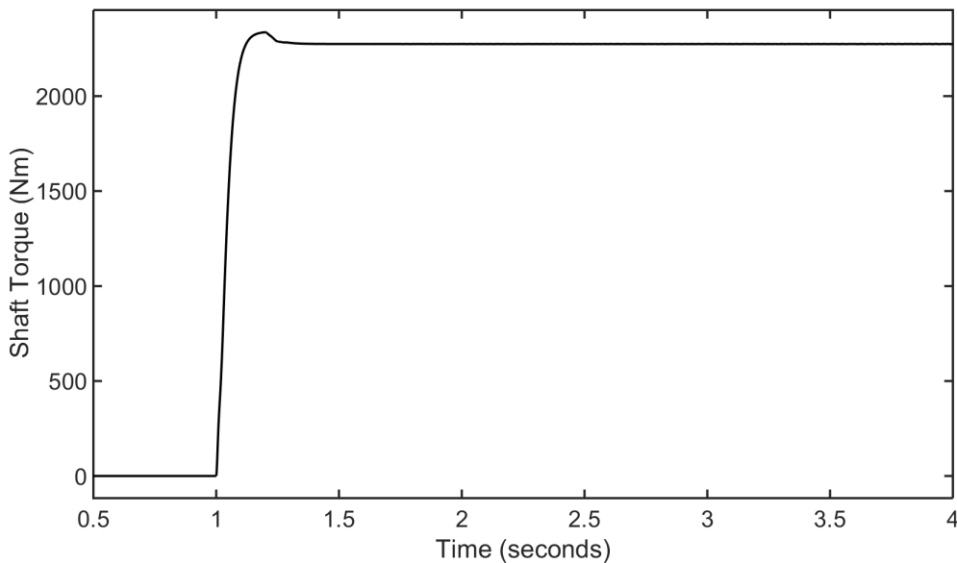


Figure 28. Shaft torque when using virtual physical damper and wheel speed estimator.

The estimated values of the states of the system, i.e shaft torsion, motor angular speed, wheel angular speed, and also shaft torque were compared with those of actual values from the plant. The plots in Figure 29-Figure 32 show both the

estimated values (dotted lines) and actual values of states from plant model (solid lines) and it can be seen that the estimated values are tracking the real values very effectively. It can be noted that since the estimator is tuned to be highly dependent on the motor speed as reference, the motor speed state is estimated as good as the real values. Even though there is a small deviation in wheel speed estimation in the beginning, since the estimator is also tuned to have its poles to the farther side in the left plane leading to fast response, it helps the deviated wheel speed to get back into correct trajectory.

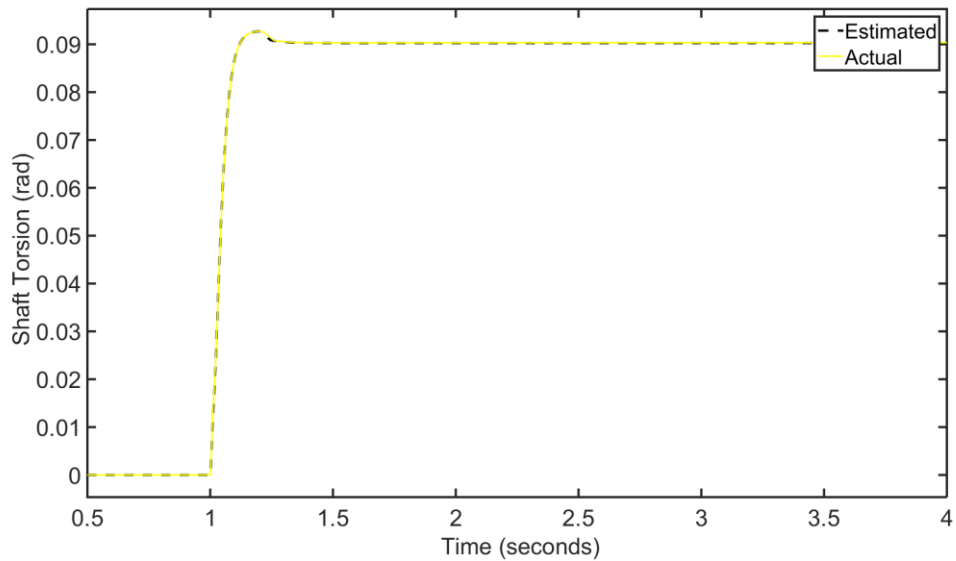


Figure 29. Shaft torsion estimated vs. real plant values.

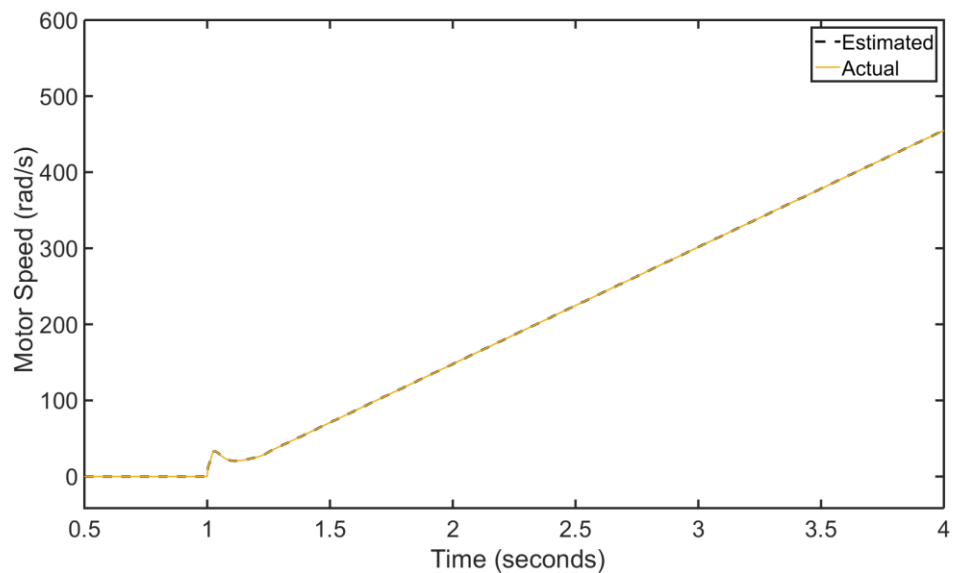


Figure 30. Motor speed estimated vs. real plant values.

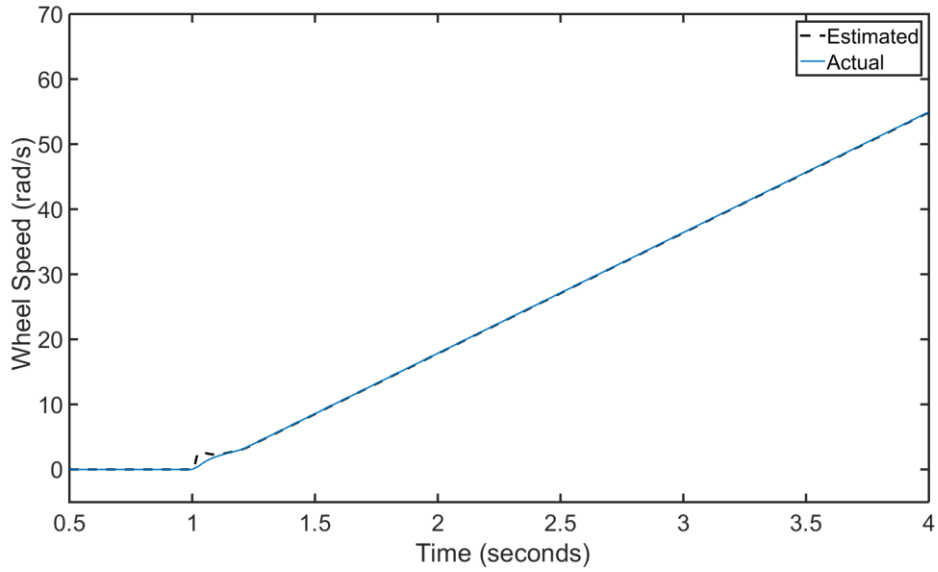


Figure 31. Wheel speed estimated vs. real plant values.

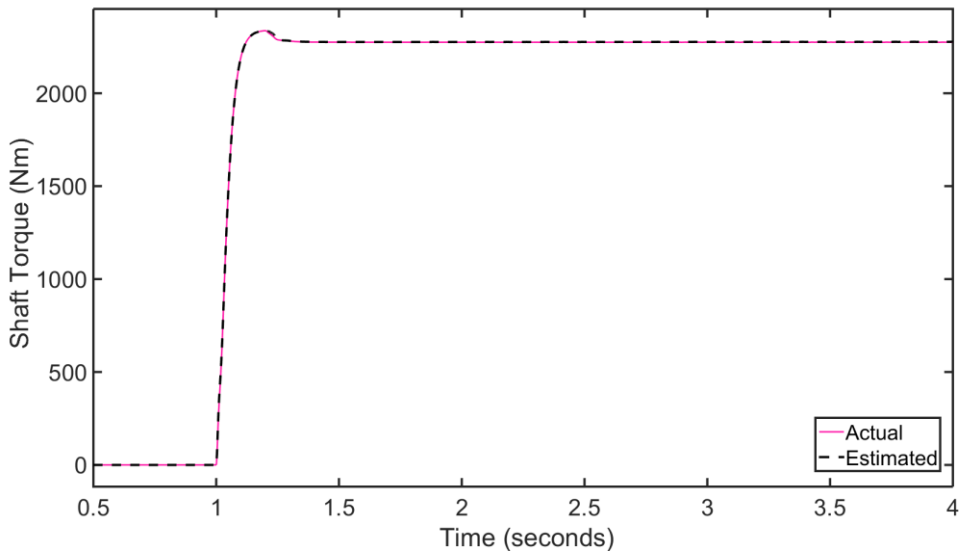


Figure 32. Shaft torque estimated vs. real plant values.

5.7 Performance Comparison of Physical Damper with Sensor and Estimator

To compare the performance between virtual physical damper using wheel speed sensor and using estimator shaft torque and rate of shaft torque were chosen as comparing parameters. A step input of 287 Nm was used as requested torque.

In case of shaft torque, the evaluation was done based on how quick the system reaches a 90% of peak torque even after the influence from the controllers, and in case of rate of shaft torque as an evaluation criteria, the controllers were compared for how quick the rate of shaft torque falls down to the value of 500.

Table 1. Time taken for the shaft torque to rise 90% of the peak.

Controller	Rise time to 90% shaft torque [seconds]
Physical damper using wheel speed sensor	0.84
Physical damper using estimator	0.09

Table 2. Time taken for the rate of shaft torque to fall down below the value 500.

Controller	Time for rate of shaft torque to reach 500 [seconds]
Physical damper using wheel speed sensor	1.746
Physical damper using estimator	0.163

From Table 1 and Table 2 it can be concluded that the virtual physical damper using estimator for state values is performing with faster response time and improved damping as the rate of shaft torque is dropping quickly, which means faster oscillations damping.

5.8 Comparison of Estimators of Two Different Approaches

A comparison was also done on two types of estimator approaches. First approach in which only motor speed is used as reference sensor signal with assumption being the data is of high reliability and less noisy. Second approach in which both wheel speed and motor speed are used as reference sensor signals with assumptions being motor speed signal data is of high reliability and less noise, wheel speed signal data is of lower frequency and more noise compared to motor speed data. For this simulation a step input of 287 Nm was used as requested torque. Figure 33 visualizes the input signal to the motor when the virtual physical damper controller using a wheel speed signal from an estimator is implemented, and the estimator uses two reference signals.

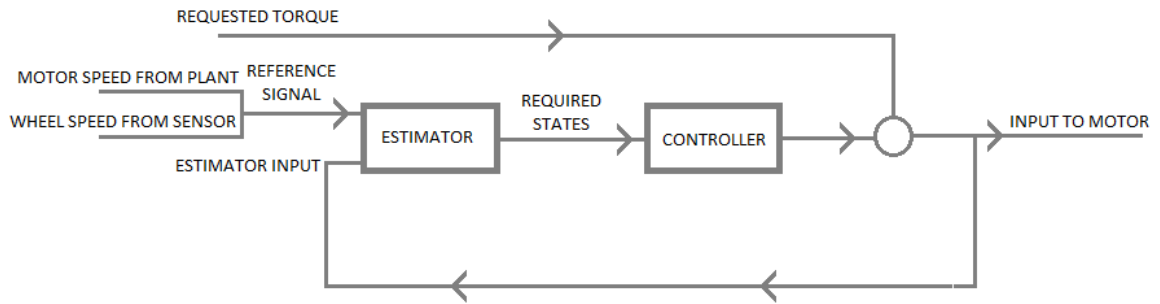


Figure 33. Estimator with two reference signals.

The plots in Figure 34-Figure 37 show that both the estimator approaches are providing good results, but the work is continued with using only motor speed as reference sensor signal in order to have less parameters to tune.

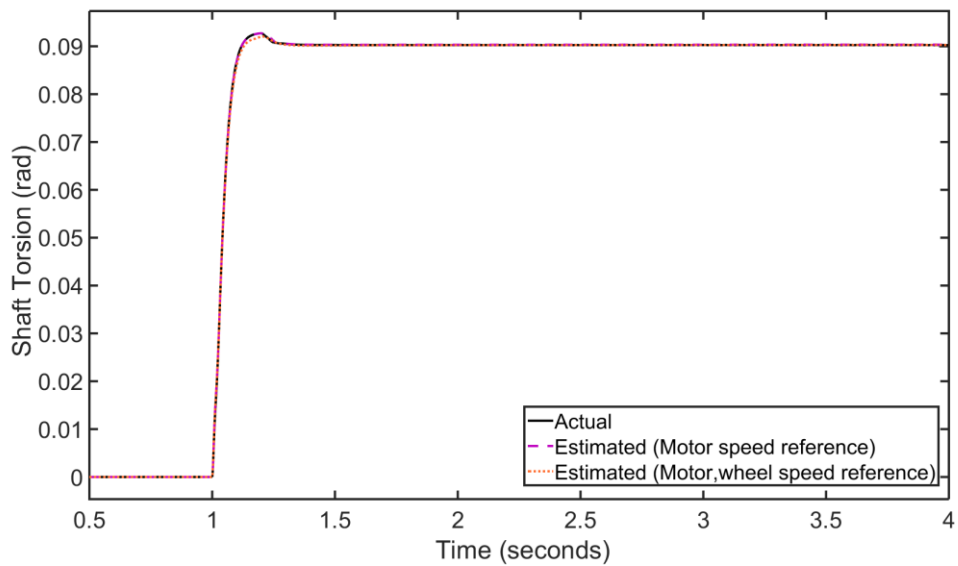


Figure 34. Shaft torsion comparison.

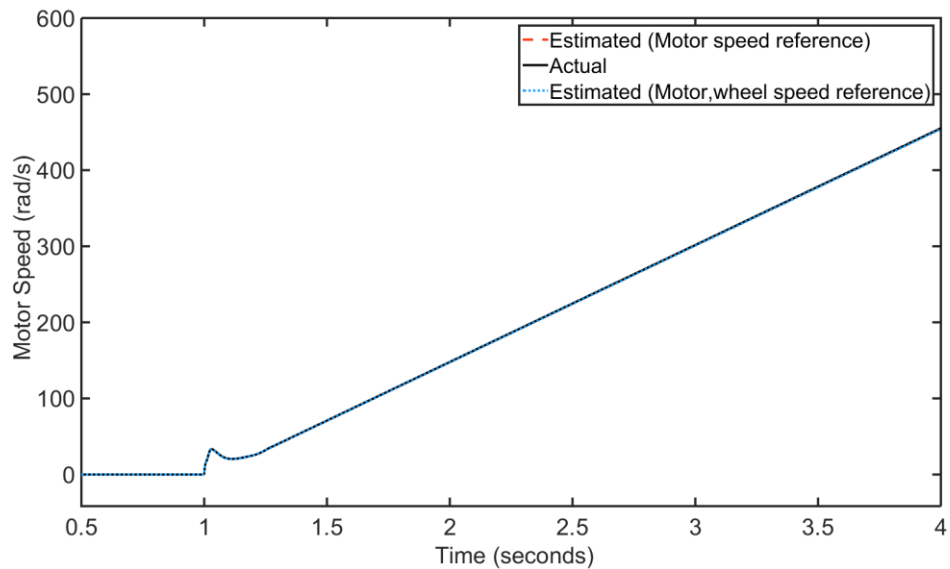


Figure 35. Motor speed comparison.

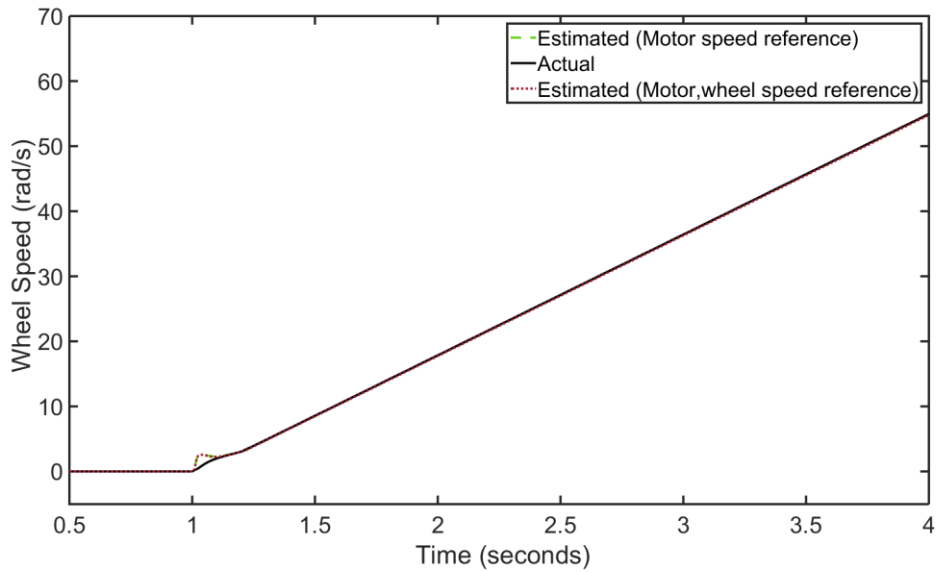


Figure 36. Wheel speed comparison.

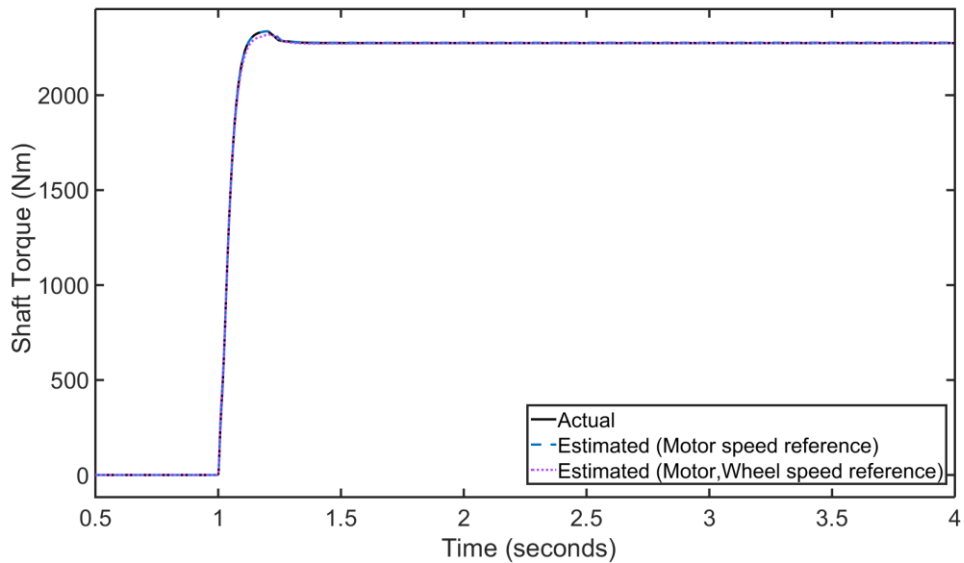


Figure 37. Shaft torque comparison.

5.9 Robustness Analysis of Estimator

As there can always be discrepancies in the parameters used for the design of controllers and estimators as they might not be same as the real values due to several factors like components replacement, change in payload, wear and tear of components, mistakes in parameter estimation etc. In order to evaluate the effects on performance of estimator the percentage error of the estimated values of motor and wheel speed with respect to the real plant values were compared by changing three different parameters. In all the cases a step input of 287 Nm was used as the requested torque.

5.9.1 Vehicle Mass

Vehicle mass here represents the entire mass of the vehicle, passenger, trailer (if any), and other payloads. Intuitively this is a parameter that can change constantly and unpredictable with large differences depending on the need of the user. So simulations were performed for two more cases with mass in the plant model increased by 50% and decreased by 50% with respect to a reference mass 'M'. Figure 38 show the motor speed estimate error from varying the vehicle mass and Figure 39 shows the wheel speed estimate error from the applying the same variation.

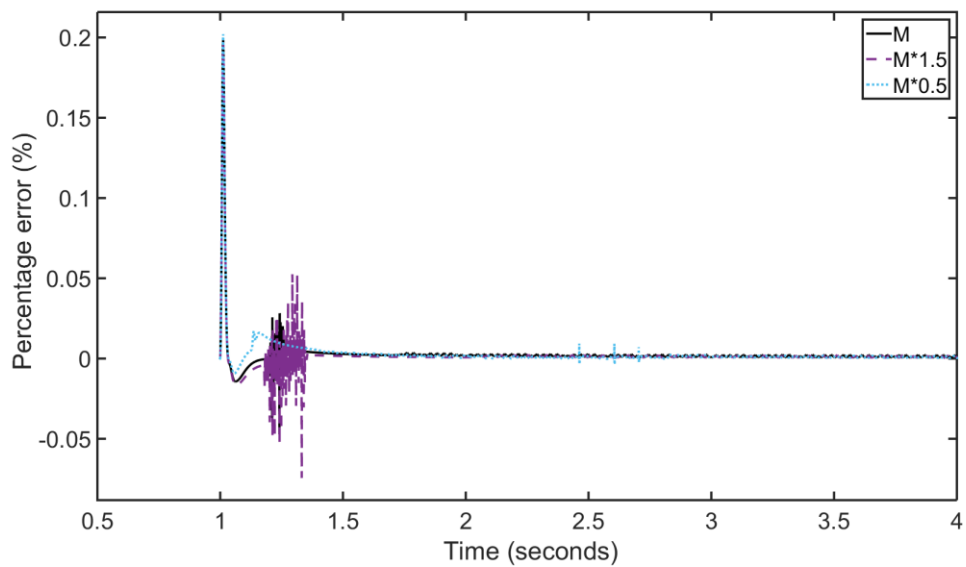


Figure 38. Motor speed estimate error.

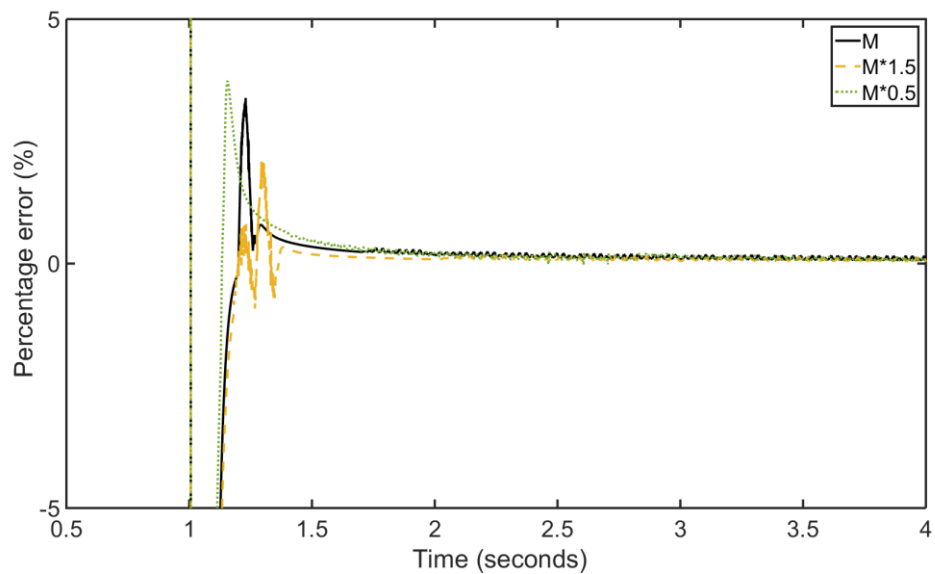


Figure 39. Wheel speed estimate error.

5.9.2 Shaft Stiffness

Shaft stiffness is also a crucial parameter which will have huge factor on the estimator and controller behaviour as it directly proportional to torque on driveshaft that reflects the oscillations. Simulations were performed for two more cases with shaft stiffness in the plant model increased by 25% and decreased by 25% with respect to a reference shaft stiffness ' K_s '. Figure 40 shows the motor speed estimate error for a shaft stiffness variation and Figure 41 shows the wheel speed estimate error from varying the same variation.

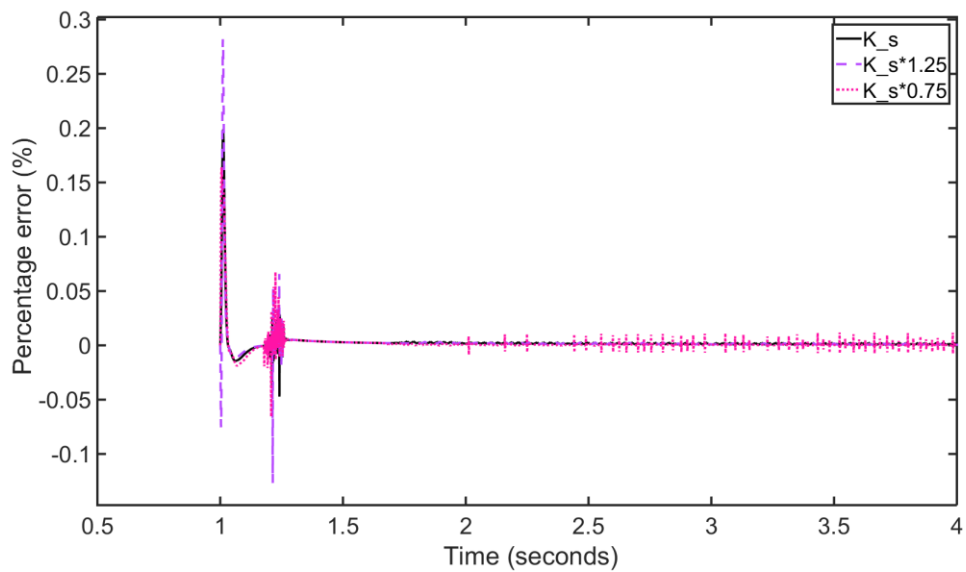


Figure 40. Motor speed estimate error.

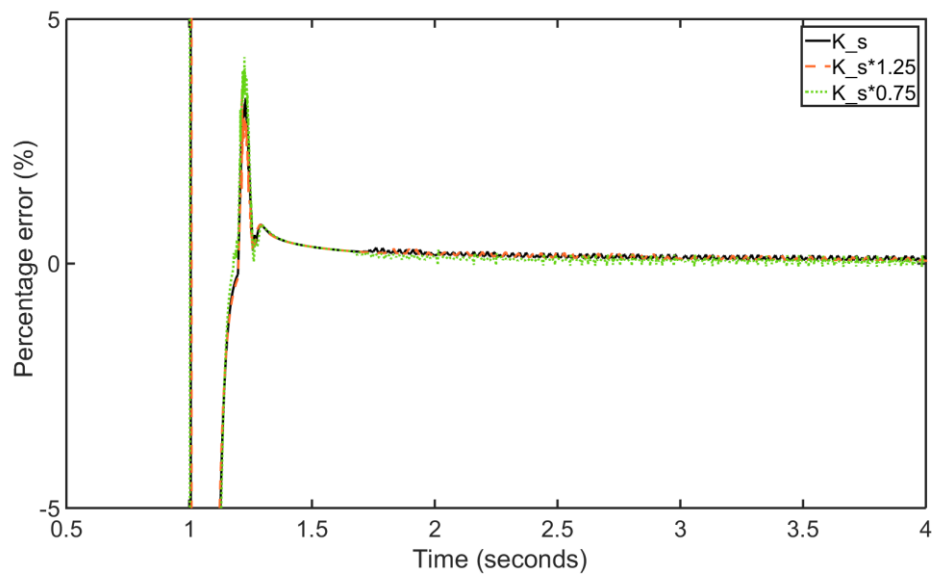


Figure 41. Wheel speed estimate error.

5.9.3 Motor Inertia

As the estimator in particular is highly dependent on the motor speed sensor data, also LQR controller dampens the oscillations by using motor input torque as control signal. Since the motor inertia is the first parameter that will have huge effect it is reasonable to consider this as a parameter of interest for assessing robustness of controllers and estimators. Since the inertia values are easily obtainable compared to other parameters like stiffness and damping coefficients a smaller range of deviation was chosen for motor inertia. Simulations were performed for two more cases with motor inertia in the plant model increased by 5% and decreased by 5% with respect to a reference motor inertia ' J_m '. Figure 42 shows the motor speed estimate error from varying the motor inertia and Figure 43 shows the wheel speed estimate error from applying the same variation.

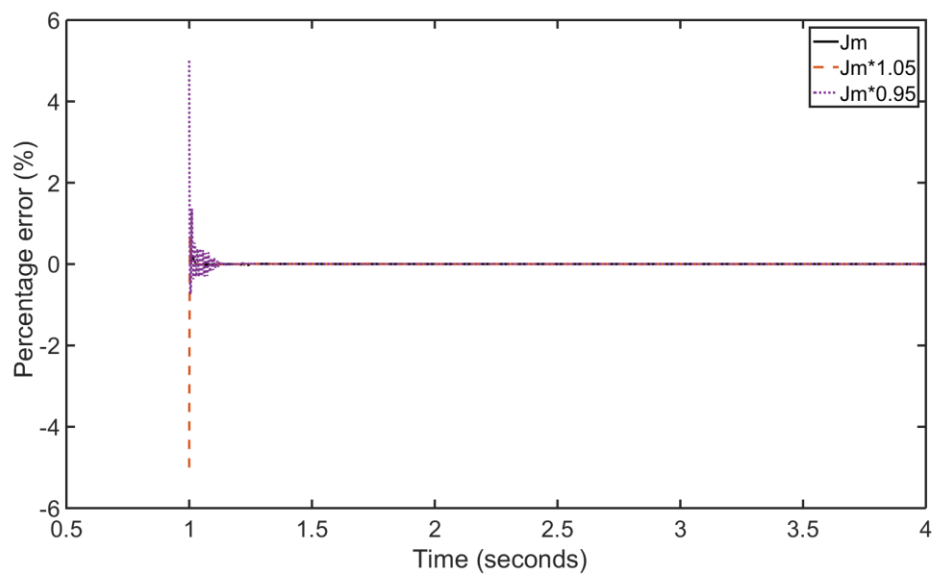


Figure 42. Motor speed estimate error.

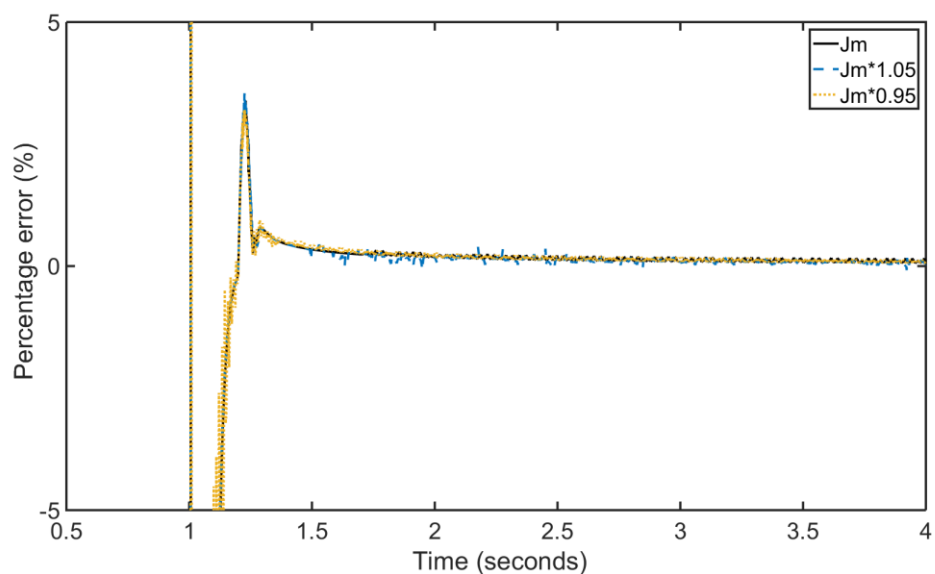


Figure 43. Wheel speed estimate error.

In all the cases above percentage errors of the estimated values have stayed quite close to zero (also the percentage errors of the reference estimator with correct parameter values). In the case of change in mass parameter, the percentage error of the estimated wheel speed converged to zero at a slower rate, but the error values were not significantly large. Also it was noticed that a peak in the initial estimate error was seen in case where the motor inertia parameter was changed.

5.10 Powertrain Model with LQR Controller

The virtual physical damper was replaced by an LQR, which gave a feedback torque based on penalizing the states in the powertrain state space model. The simulation of the model for a step torque input of 287 Nm resulted in a driveshaft torque response presented in Figure 44. The graph shows that there are still oscillations in the initial phase of the step input. These are clearly less oscillations than for the non-controlled powertrain model, but the performance of the LQR seems to be worse than the performance of the virtual, physical damper. Another drawback for the LQR is that the torque at which the driveshaft is stabilizing is less than for the non-controlled model. The model with the LQR is stabilized at 2006 Nm, while the non-controlled model as well as the model with virtual, physical damper are both stabilized at 2333 Nm. The torque loss is due to that the LQR keeps on regulating the EM with a feedback torque even after the driveline is stabilized. This is a result of the LQR control strategy, to minimize cost function based on the states of the model that are penalised. In this case the penalised state was the torsion in the driveshaft. Hence the LQR tries to minimize the torsion in the driveshaft, which is directly related to the torque on the shaft. This is why the controller keeps on sending a feedback torque even after stabilizing the driveline.

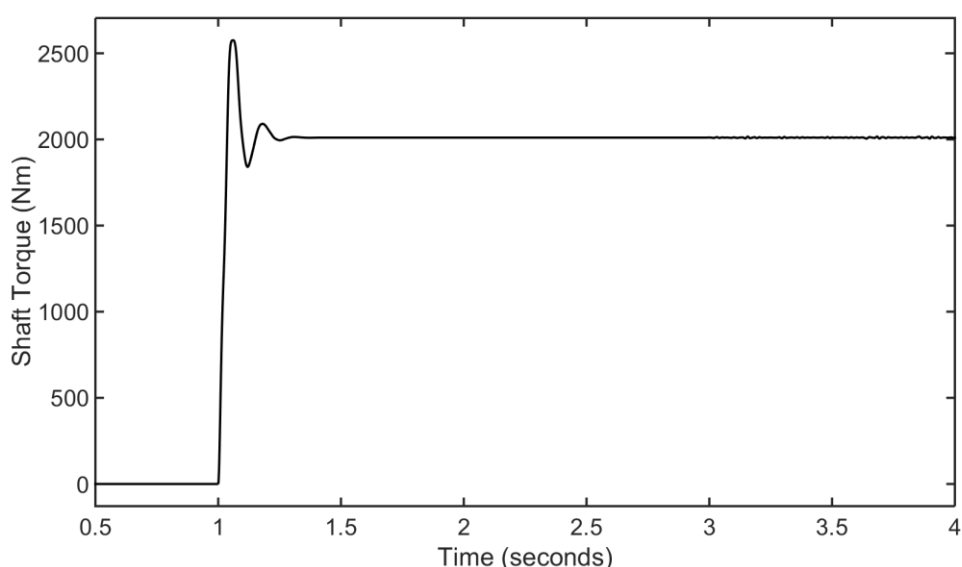


Figure 44. Shaft torque for a step input of 287 Nm for the powertrain model with a feedback torque generated by the LQR.

The results from the model with LQR opted for another approach, using the LQRY controller, why from hereon, the results will mainly source from the powertrain

model combined with an LQRY controller. See section 4.4 for a more detailed explanation.

5.11 Powertrain Model with LQRY Controller

The LQR controller results showed that the strategy to penalise shaft torsion is not favourable, so an LQRY controller, which in contrast to the LQR controller minimizes the outputs from the state space model, making it possible to have the controller penalize the rate of shaft torsion instead of the shaft torsion was chosen. Running the powertrain model with an LQRY controller results in a much better stabilization of the driveline compared to running with the LQR. The driveshaft torque response for a step input of 287 Nm is visualized in Figure 45. The performance seems to be very similar to the performance of the model with a virtual physical damper. There are no visible oscillations. The stabilization torque on the driveshaft is 2333 Nm as for the non-controlled model and the model with virtual physical damper.

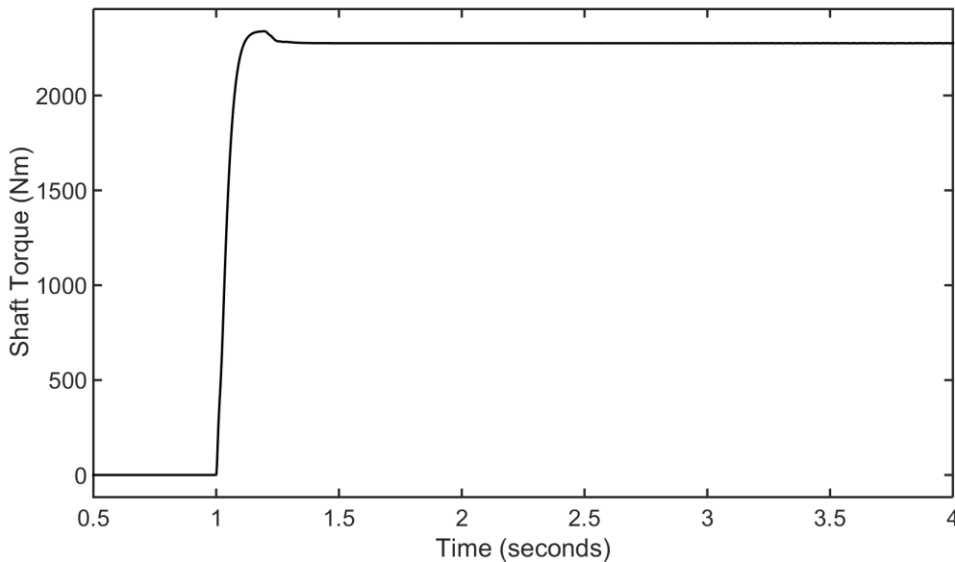


Figure 45. Shaft torque for a step input of 287 Nm for the powertrain model with a feedback torque generated by the LQRY.

5.12 Performance Comparison of Physical Damper with Estimator, LQR and LQRY

To compare the performance between virtual physical damper, LQR and LQRY the estimators were removed and the required states were directly taken from the plant. This was done so that the performance from pure controller stand point could be compared. For this, a similar approach was used as that in section 5.7 along with time to reach a speed of 60km/h as an extra parameter to compare. In case of shaft torque, the evaluation was done based on how quick the system reaches a 90% of peak torque even after the influence from the controllers, and in case of rate of shaft torque as an evaluation criteria, the controllers were compared for how quick the rate of shaft torque falls down to the value of 500. A step input of 287 Nm was used as requested torque.

Table 3. Time taken for the shaft torque to rise 90% of the peak.

Controller	Rise time to 90% shaft torque [seconds]
Physical damper	0.09
LQR	0.037
LQRY	0.086

Table 4. Time taken for the rate of shaft torque to fall down below the value 10.

Controller	Time for rate of shaft torque to reach 500 [seconds]
Physical damper	0.163
LQR	0.29
LQRY	0.153

Table 5. Time taken for vehicle to reach speed of 60 km/h.

Controller	Time to reach 60 km/h [seconds]
Virtual physical damper	5.82
LQR	6.283
LQRY	5.82

Looking at Table 4, LQR is lagging in terms of stabilizing fast enough, with LQRY being fastest followed by virtual physical damper. But Table 3 shows that the system using LQR reaches 90% of peak shaft torque much faster. This is due to the oscillations which overshoot the peak, leading to much faster rise time in the beginning. Hence, to get a better picture at this comparison, time to reach a vehicle

speed of 60 km/h is also evaluated, and for sure looking at Table 5 explains that LQR leads to slower system response compared to the other two control strategies.

5.13 Robustness Analysis of Virtual Physical Damper and LQRY with Estimator

To check for robustness of the controllers when working along with the estimator similar strategy is used as that of section 5.9 and varying mass, shaft stiffness and motor inertia in the plant model, using a step input of 287 Nm as requested torque.

5.13.1 Vehicle Mass

Three cases were performed, one with a reference mass and the other two are performed by increasing and decreased the mass of the vehicle by 50% with respect to a reference mass 'M'. Figure 46 shows the effect on shaft torque for the model using virtual physical damper, and Figure 47 for the model using LQRY controller, from varying the vehicle mass.

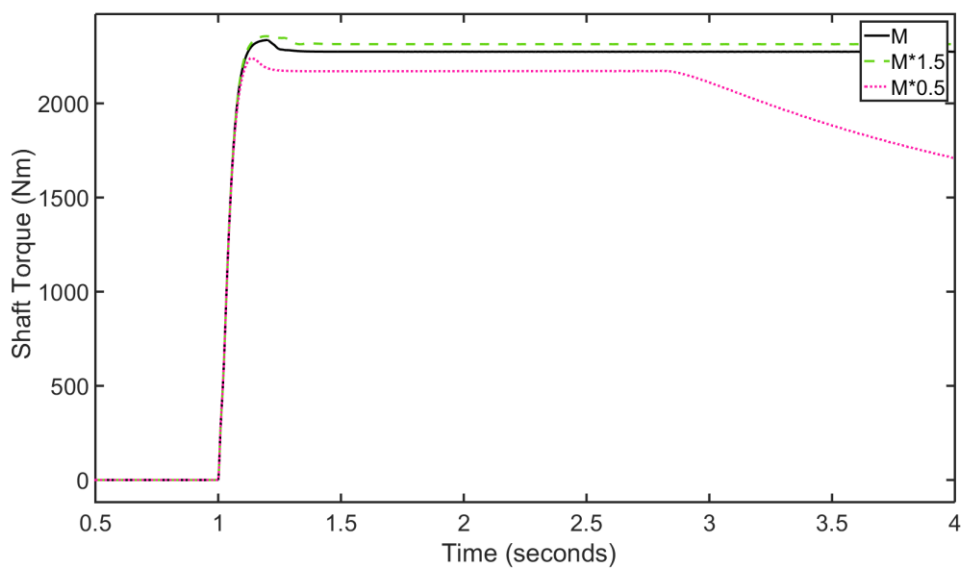


Figure 46. Effect on shaft torque, virtual physical damper.

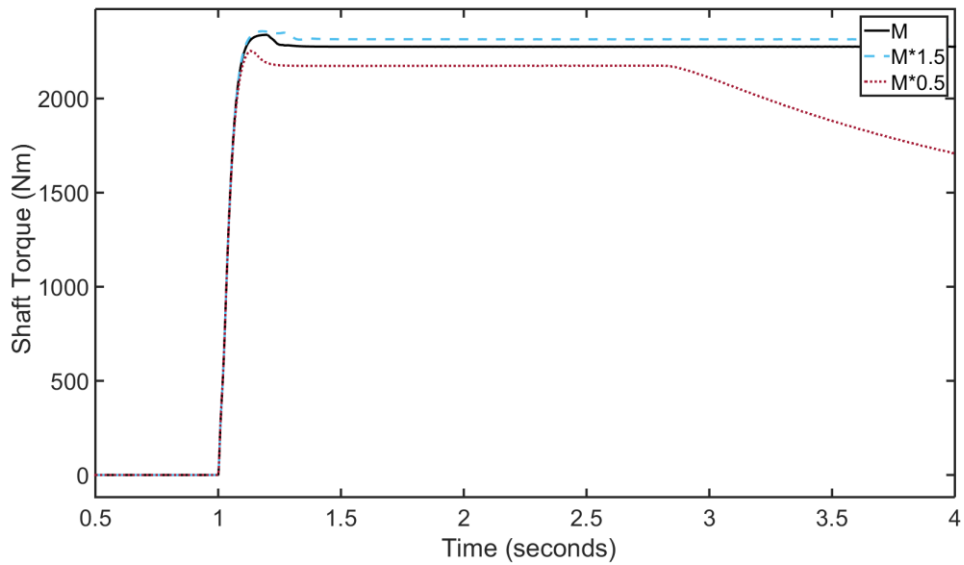


Figure 47. Effect on shaft torque, LQRY controller.

5.13.2 Shaft Stiffness

Three cases were performed, one with a reference Shaft stiffness and the other two are performed by increasing and decreased the Shaft stiffness by 25% with respect to a reference Shaft stiffness 'K_s'. Figure 48 shows the effect on shaft torque for the model using virtual physical damper, and Figure 49 for the model using LQRY controller, from varying the shaft stiffness.

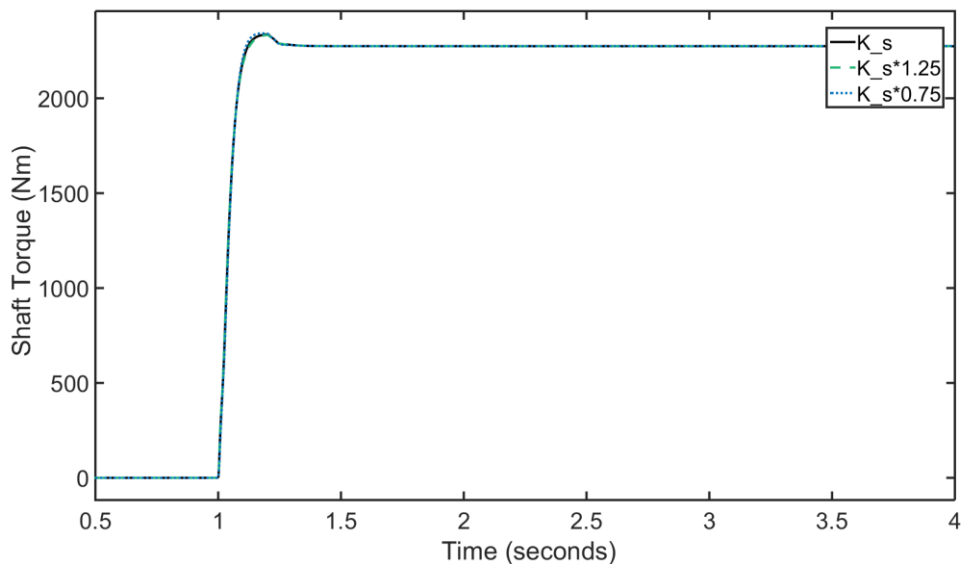


Figure 48. Effect on shaft torque, virtual physical damper.

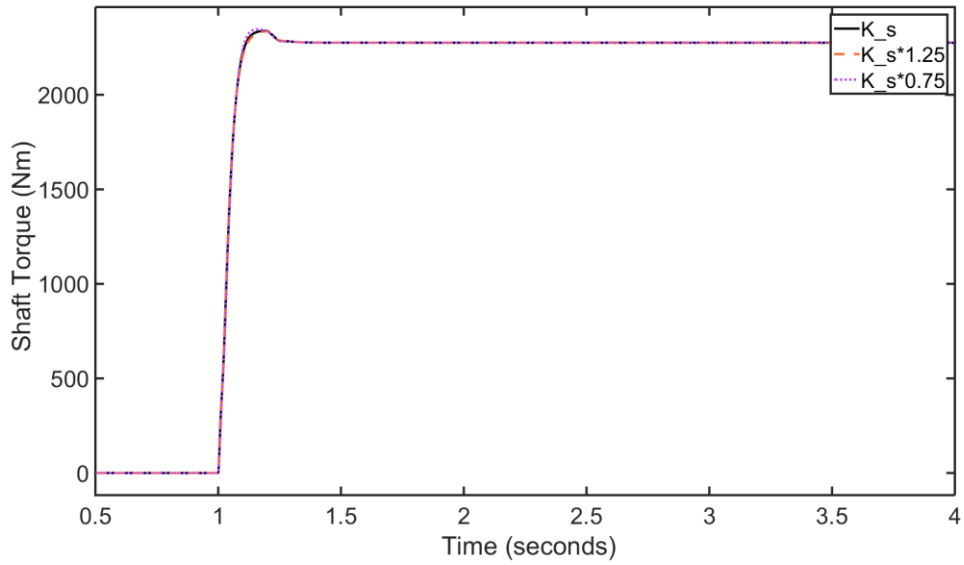


Figure 49. Effect on shaft torque, LQRY controller.

5.13.3 Motor Inertia

Three cases were performed, one with a reference motor inertia and the other two are performed with an increased and respectively decreased motor inertia by 5% with respect to a reference motor inertia 'Jm'. Figure 50 shows the effect on shaft torque for the model using virtual physical damper, and Figure 51 for the model using LQRY controller, from varying the motor inertia.

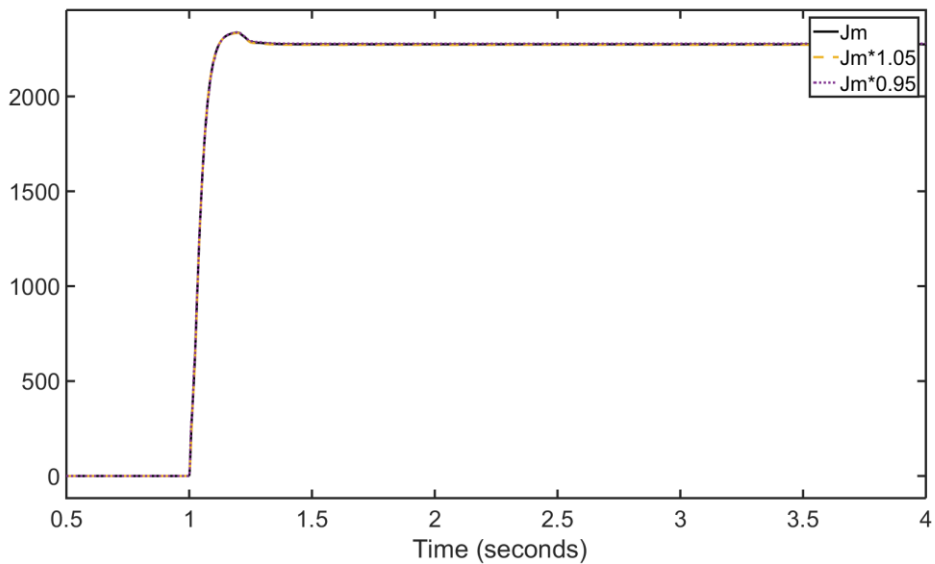


Figure 50. Effect on shaft torque, virtual physical damper.

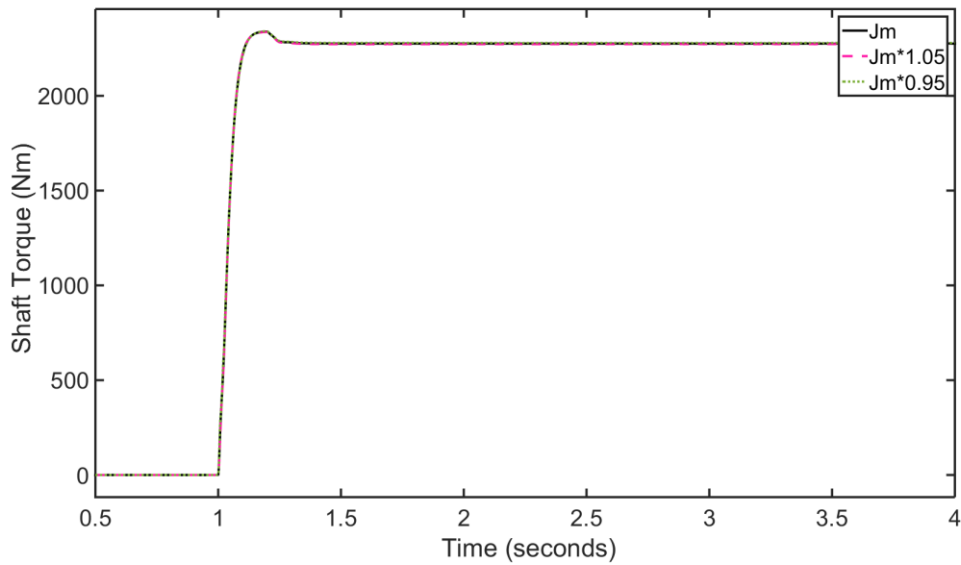


Figure 51. Effect on shaft torque, LQRY controller.

From all the above cases it can be seen that the controllers were able to handle discrepancies quite well.

5.14 Effect from Backlash in the Model

Since the backlash is an imminent non-linearity in a real vehicle, adding to the concerns about the controllers and estimator performance a simulation was performed for a requested torque of 287 Nm and a backlash of 30 degrees which is the lumped value of all the backlashes in the powertrain until the wheels to verify the effect from backlash in the plant model. This was added right before the driveshaft in the plant model. Figure 52 shows the effect on shaft torque from backlash for the model using virtual physical damper with and without estimator and for the model using LQR with estimator. Figure 53 shows the effect on torque input after control from backlash for the model using virtual physical damper with and without estimator and the model using LQRY controller.

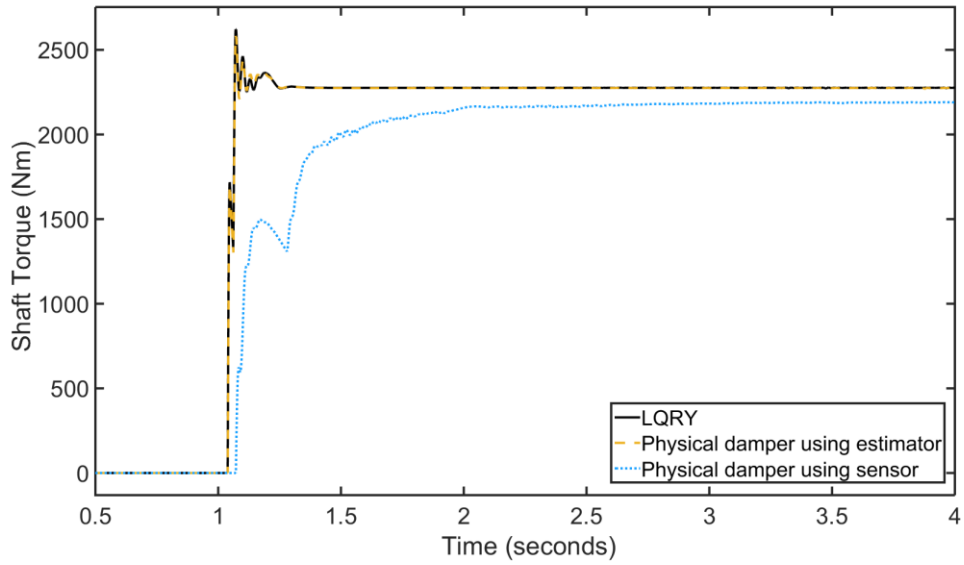


Figure 52. Effect of backlash inclusion in the plant model.

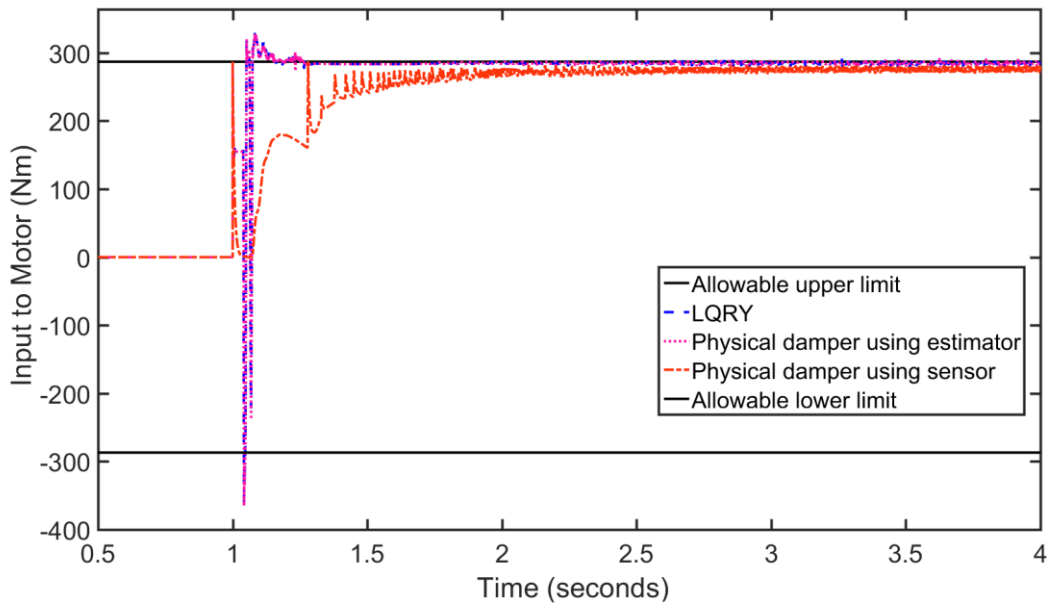


Figure 53. Effect on torque input after control due to backlash.

From the plot in Figure 52 it can be seen that the physical damper and LQRY using estimator are effected due to non-linearity introduction, also physical damper using sensor data plot looks to have longer stabilizing time than it was before the backlash implementation.

Another concern that comes up after implementation is that looking from plot Figure 53 it is evident that the backlash is also leading the controller to improvise torque values which are out of the limits. So to overcome this a torque controller was also implemated whose results are discussed in section 5.15.

5.15 Torque Saturation

As mentioned about the necessity for torque saturation in section 5.14 it was implemented after the controllers to limit the torque from the controllers. For testing its effect a step input of 287 Nm was used as requested torque signal. Figure 54. Controller with torque saturation shows the layout of the powertrain model with torque saturation.

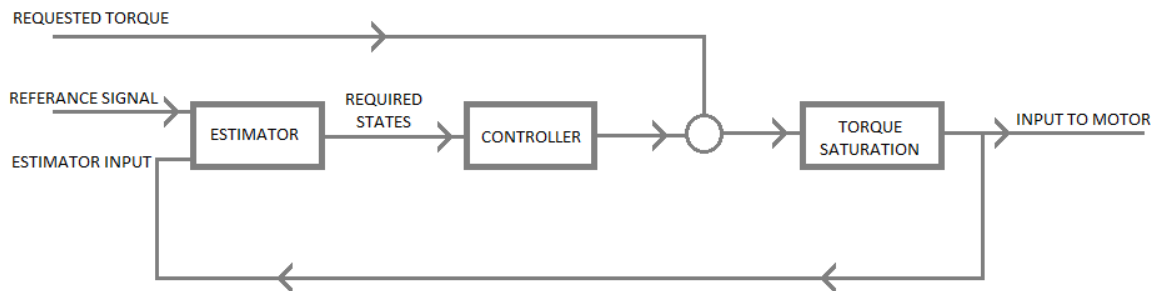


Figure 54. Controller with torque saturation.

Looking at the plot in Figure 55 it can be seen that the torque limiting strategy is able to restrict the torque after the controllers within the allowable region. But at the same time its effect can be seen on the shaft torque in the plot in Figure 56 where the model with unsaturated control has a smoother trajectory towards stabilizing compared to the model which has torque saturated control.

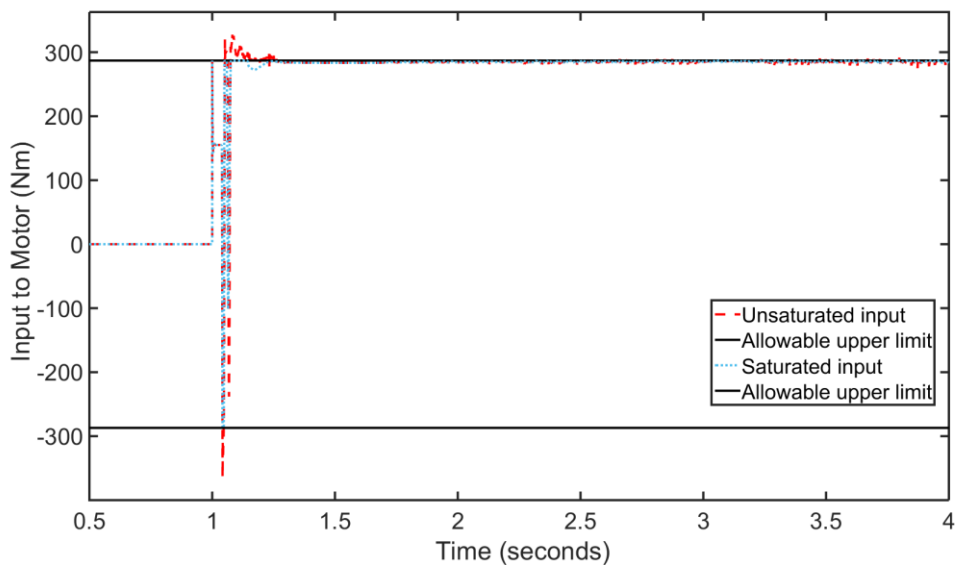


Figure 55. Effect of torque saturation on input to motor for physical damper with estimator.

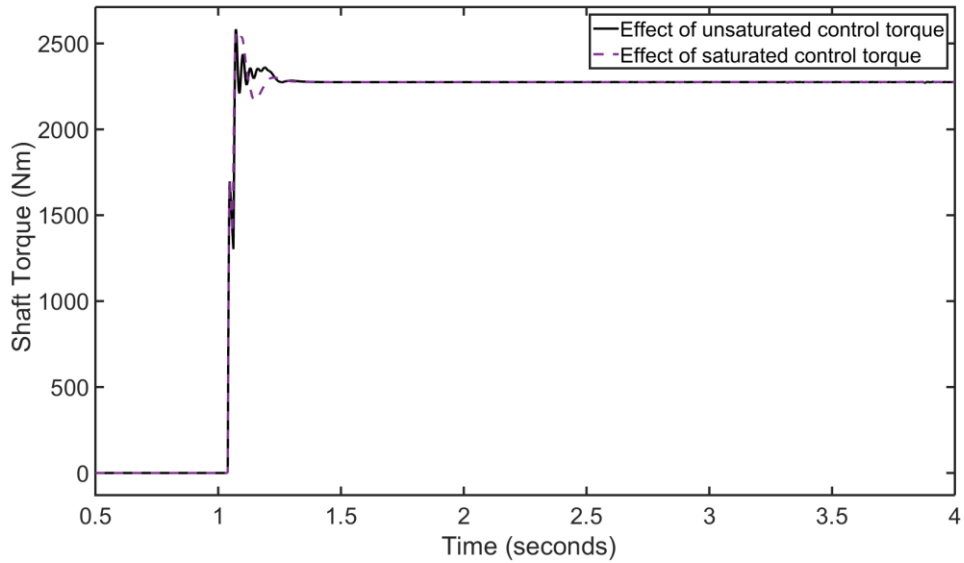


Figure 56. Effect on shaft torque due to saturated and unsaturated effective control torque.

5.16 Effect of Backlash Controller for Various Controllers

After simulating the plant model with backlash and observing the effect on the controllers a backlash controller was developed and implemented, as mentioned in section 4.7, to bypass the controllers through the non-linear region. A step input of 287 Nm was used as requested torque signal. Figure 57 shows a layout of the powertrain model with backlash controller.

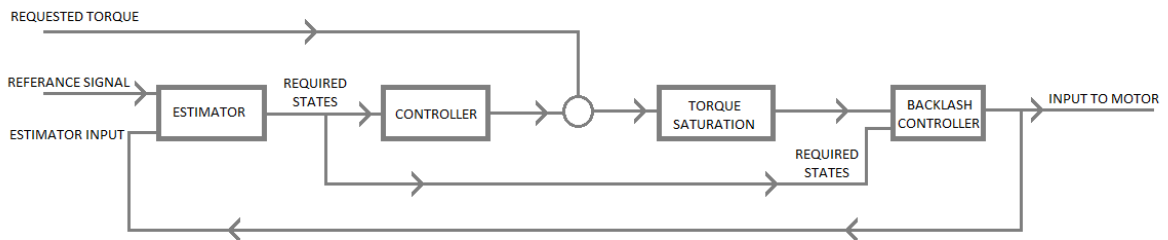


Figure 57. Complete control with backlash controller included.

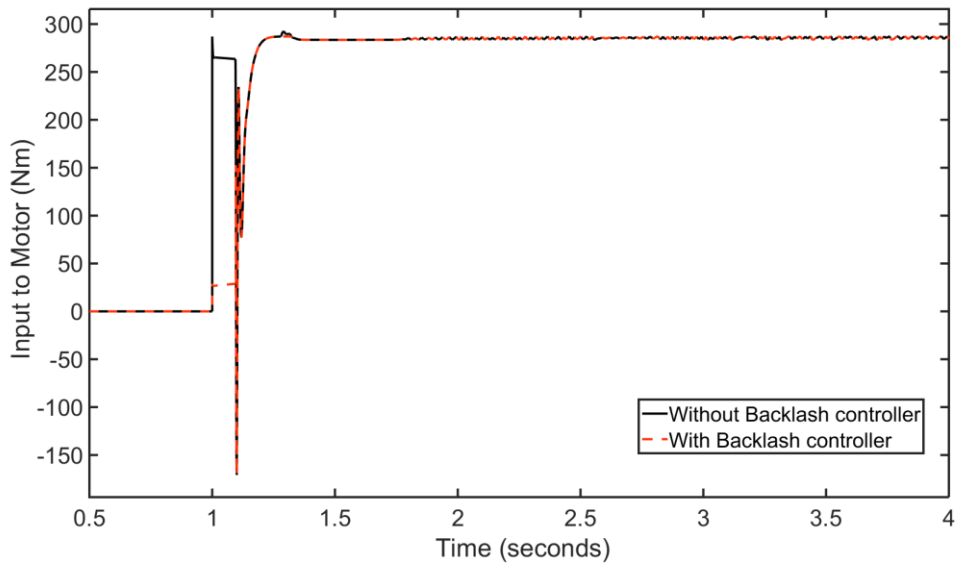


Figure 58. Controller torque for the model with physical damper with estimator, with and without backlash control.

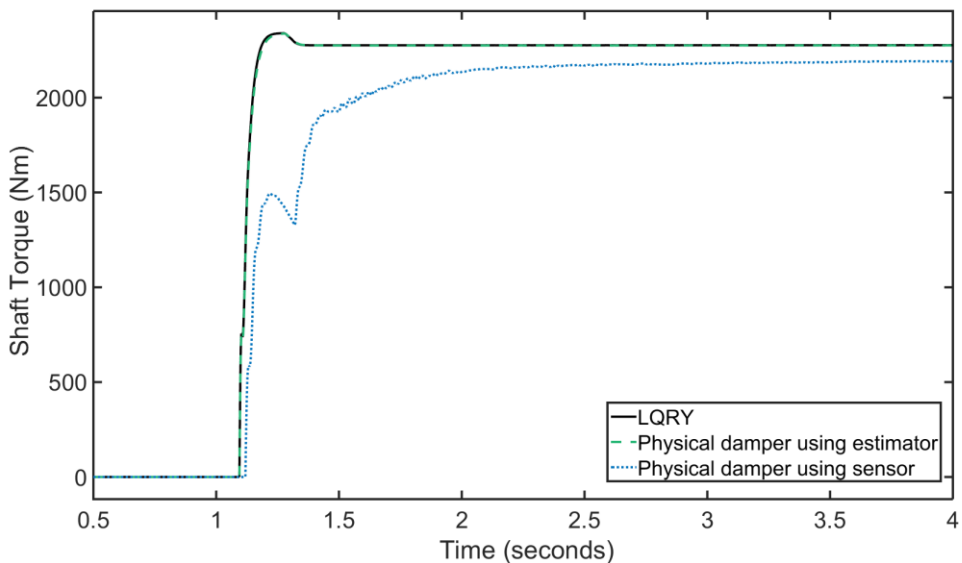


Figure 59. Effect of backlash controller for various controllers.

By looking at the plot in Figure 58, we can see that the input torques with and without using the backlash controller are quite distinctive. Also from the plot in Figure 59 the shaft torque looks smoother for the case of virtual physical damper with estimator and LQRY with estimator. However the virtual physical damper using wheel speed data from sensor does not improve in the oscillation damping.

Also a performance comparison was done in a similar way to that in section 5.12. In case of shaft torque, the evaluation was done based on how quick the system reaches a 90% of peak torque even after the influence from the controllers, and in case of rate of shaft torque as an evaluation criteria, the controllers were compared for how quick the rate of shaft torque falls down to the value of 500. A step input of 287 Nm was used as requested torque.

Table 6. Time taken for the shaft torque to rise 90% of the peak.

Controller	Rise time to 90% shaft torque [seconds]
Physical damper sensor	0.94
Physical damper estimator	0.163
LQRY	0.16

Table 7. Time taken for the rate of shaft torque to fall down below the value 100.

Controller	Time for rate of shaft torque to reach 500 [seconds]
Physical damper sensor	1.6
Physical damper estimator	0.441
LQRY	0.44

Table 8. Time taken by the vehicle to reach 60 km/h.

Controller	Time to reach 60 km/h [seconds]
Physical damper sensor	6.23
Physical damper estimator	5.91
LQRY	5.91

Looking at Table 7, virtual physical damper using wheel speed sensor is lagging in terms of stabilizing fast enough, with LQRY being fastest followed by virtual physical damper with estimator. But in Table 6 it can be seen that the system using virtual physical damper using wheel speed sensor reaches 90% of peak shaft torque much faster and this is due to the oscillations which overshoot the peak leading to much faster rise time in the beginning. So the time for the vehicle to reach a certain speed is also looked at for this comparison to get a better picture, and for sure looking at Table 8 explains that virtual physical damper using wheel speed sensor leads to slower system response compared to the other two control strategies.

5.17 Effect Due to and on Powertrain Housing Oscillations

The PT housing is a single unit and is mounted to the chassis through elastic mounts with certain stiffness and damping coefficients. This in turn results in oscillations of the housing which are effected by the driveshaft oscillations and also can have influence on the driveshaft oscillations. Simulations were performed to check the extent of difference that can occur with requested torque being a step input of 287 Nm.

5.17.1 Effect on the Shaft Oscillations Due to Housing Oscillations

In this case the changes shaft oscillations were compared by varying the housing mount parameters. Both the stiffness and damping values were increased and decreased by a factor of 30% where ' K_h ' is housing mount stiffness and ' C_h ' is housing mount damping. All the simulations were performed on the plant model without any controller to be able to see the effects from the oscillations.

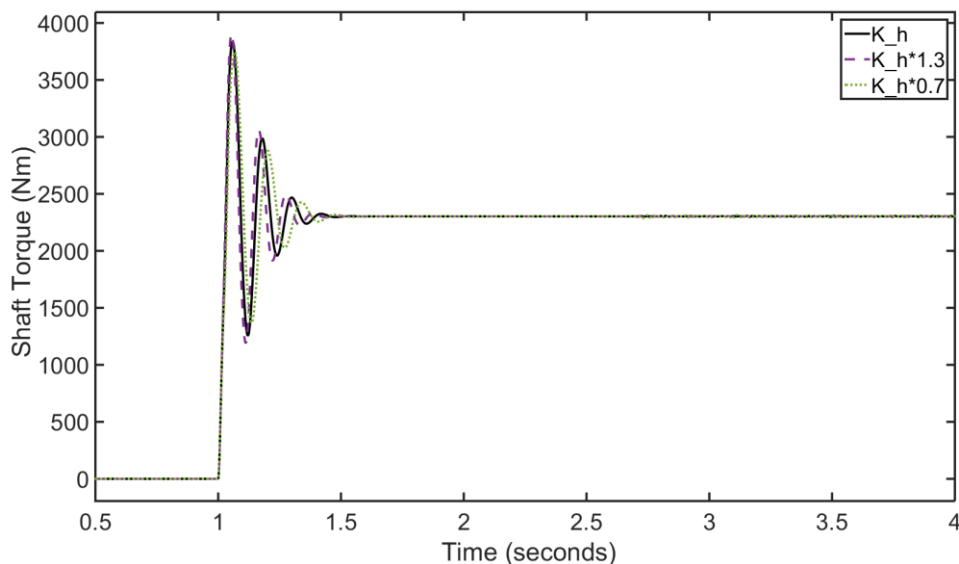


Figure 60. Effect on shaft oscillations due to varying housing mounts' stiffness.

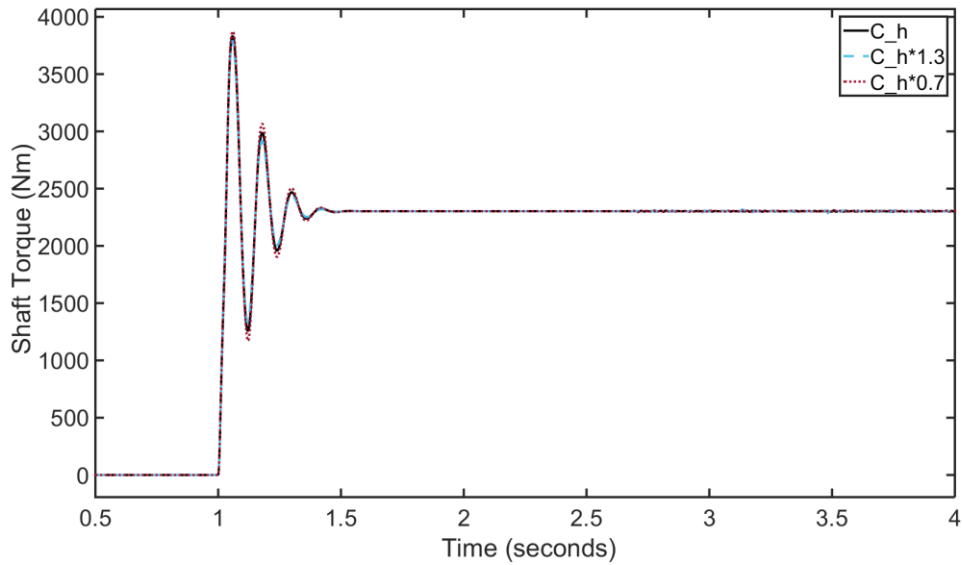


Figure 61. Effect on shaft oscillations due to varying housing mounts' damping.

From the plots in Figure 60 and Figure 61 it can be seen that changing the damping values of the powertrain housing mounts have not much effect on the oscillations of the driveshaft, but on the other hand the powertrain housing mounts seem to decrease the oscillations amplitude on a small level with decreasing stiffness. This can be due to the fact that with lesser stiffness of the mounts and same torque the housing will have increased oscillations amplitude leading to subtracting of oscillations amplitude in the shaft.

5.17.2 Effect on the Housing Oscillations Due to Shaft Oscillations

In this case the influence of the shaft oscillations on the housing oscillations were compared for three cases which are: No active damping, and with active damping strategies of virtual physical damper, LQR controller.

Three cases were run:

- Case 1: No controller (pure plant model)
- Case 2: Virtual physical damper as controller
- Case 3: LQR as controller

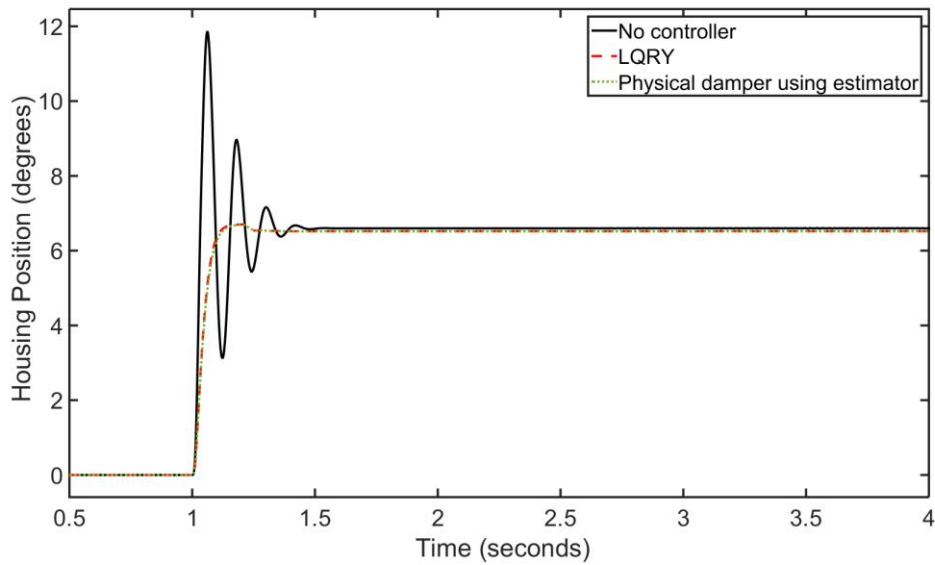


Figure 62. Effect on housing oscillations due to shaft oscillations.

In Figure 62 it can be seen that the controllers for sure help in attenuating powertrain housing oscillations because the input to the powertrain housing oscillations is the shaft torque and if the controllers damp the oscillations in the shaft, no effective oscillations will be produced in the powertrain housing. This will help in optimizing the mounts for lesser forces.

5.18 Controller Performance for Different Torque Input Levels

The controllers were also assessed for their performance with different levels of torque input to the system. In this assessment the backlash controller is also included.

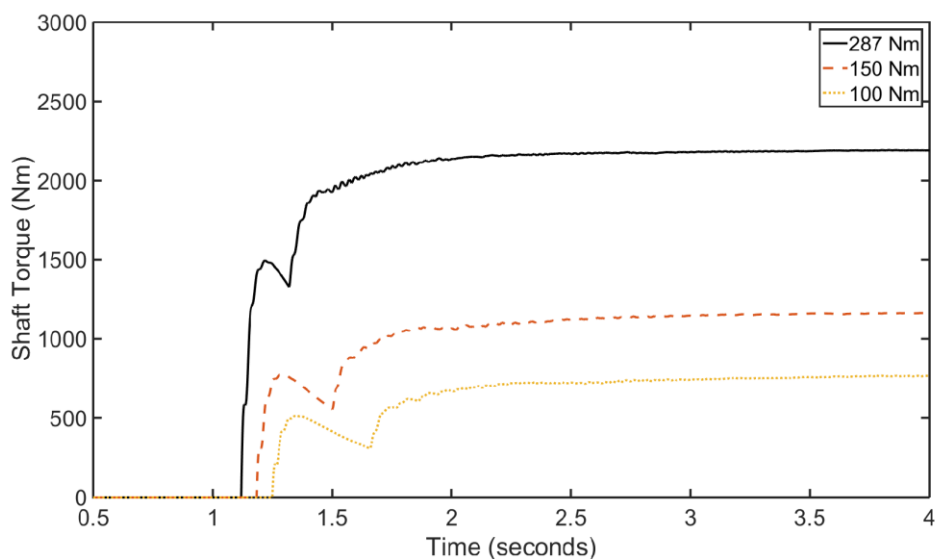


Figure 63. Shaft torque when using virtual physical damper and wheel speed sensor.

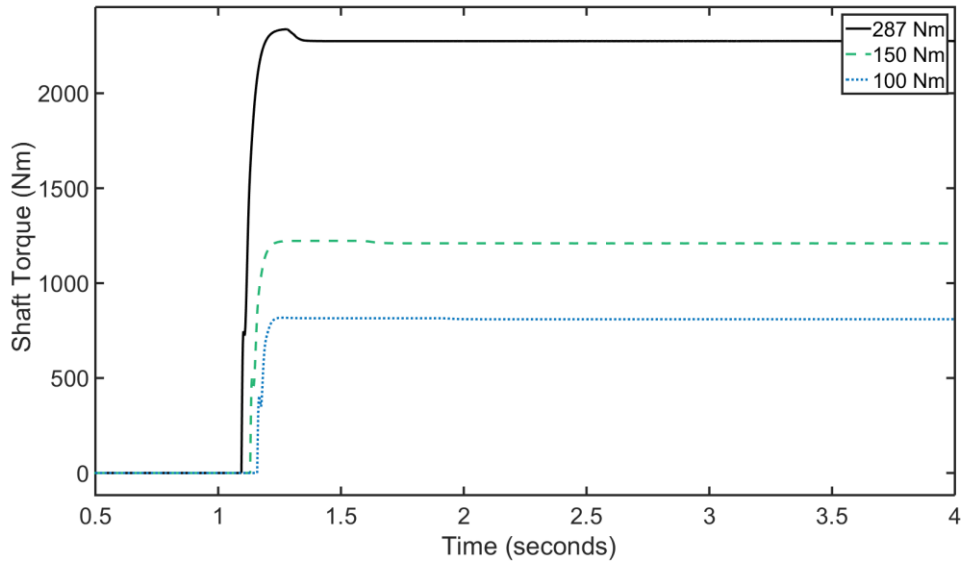


Figure 64. Shaft torque when using virtual physical damper and estimator.

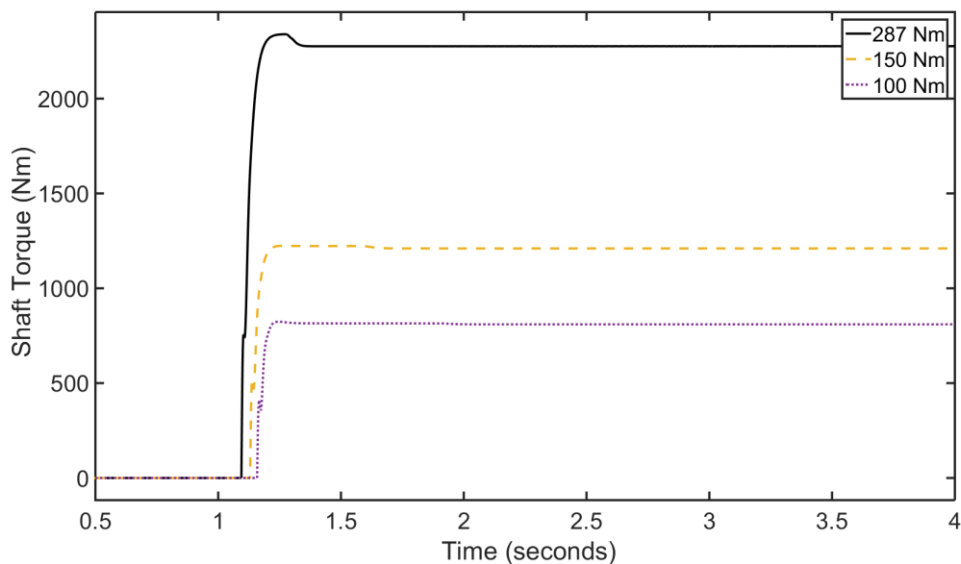


Figure 65. Shaft torque when using LQRY.

From the plots in Figure 63-Figure 65 it can be seen that both the virtual physical damper using estimator and LQRY using estimator are able to effectively dampen oscillations in a good range of torque variation, so it can be safely assumed that these damping strategies will be working for all torque input levels. But the Virtual Physical damper using wheel speed sensor is consistently having amplified issues after introduction of backlash even at smaller input torque levels.

5.19 Backlash Estimation

Backlash estimation was performed to be able to use for controlling through the backlash transition. The backlash introduced in the system was 25 degrees but the estimated value was 31.74 degrees. Also it takes long time for estimating the backlash value. The estimation plot can be seen in the Figure 66.

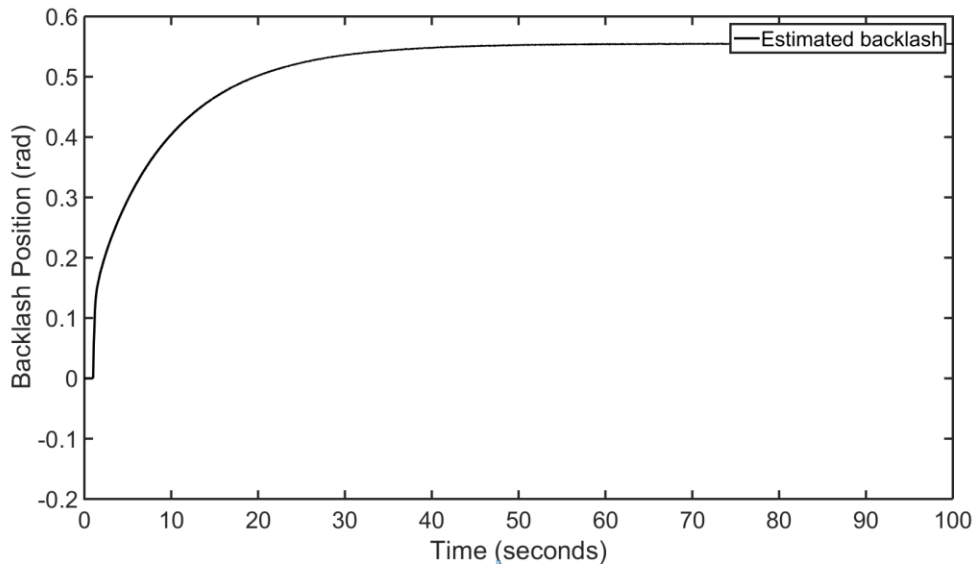


Figure 66. Estimated backlash.

One big problem for estimating backlash can be that the traversal through the backlash region happens only once and that means only one data point for the estimator to refer. This leads to the estimator to keep tracking the initial trajectory which might or might not be the correct one. The other issue can be that it takes long time for reaching the steady state value for backlash which is not favourable if we want to control the system fast enough.

6 Conclusions

The following chapter gathers the conclusions drawn from the work done within the scope of the thesis, as listed below:

- Plant simulations show that there is a significant effect on the driveability due to the oscillations caused by elasticity of the driveshaft as their frequency fall in the range felt easily by humans.
- The wheel speed data from the sensor cannot be used directly for a controller to actively damp as the controller needs to provide feedback gain at high frequency for faster damping, but the wheel speed data from sensor does not have a required high resolution. This can be overcome by using estimator or applying filters.
- For the current state space model used for estimator having good quality motor speed signal as reference is sufficient enough to estimate all three states (shaft torsion, motor speed, wheel speed) with good accuracy which can be further used for calculating shaft torque. This will help in having less parameters to tune for estimator.
- Using estimator for Virtual Physical damper is a good way to have better controller performance when compared to that of Virtual Physical damper which uses wheel speed sensor data.
- The developed estimator has good stability even when parameter discrepancies are introduced in the plant model.
- Using speed difference at shaft ends (rate of shaft torsion) is a better criteria to relate to shaft oscillations for controller to use as a reference for active damping than using shaft torsion (On the other hand referring to shaft torsion can be a better strategy to damp shaft oscillations during gear shifting for instance).
- Both the controller (Virtual Physical damper and LQRY using estimator) have good stability even when parameter discrepancies are introduced in the plant model.
- In terms of performance LQRY is able to damp oscillations quicker and has faster rise time than Virtual Physical damper. But when looking from the vehicle velocity point of view they do not have much difference in times taken to reach 60 Km/h.
- Saturating the effective torque after the controller is necessary as it can request values out of the allowable limits.

- As the controllers employed here are linear in nature, non-linearity like backlash tend to have impact on its performance to some extent for which having an additional control strategy can be used to reduce this effect.
- Also the backlash controller used is able to manage the non-linearity region, but with a drawback of slower response time. This is a compromise which has to be tweaked depending on the performance required from the controller and the plant response.

7 Future Work Recommendations

This chapter suggests some work of interest that still can be performed on the topic of the thesis, listed as below:

- Further development of present plant model used can be made to incorporate differential and two wheels per axle, so that analysis can be done for the working of the controllers in case of different road friction conditions or turnings.
- Developing the powertrain housing and mount system further to have more degrees of freedom in order to investigate how much difference it would be causing.
- Developing a controller which can be used on individual wheels by having braking torque as control signal and comparing its performance with the initial controllers which on the other hand have a single control signal i.e. the motor torque to control the driveline oscillations.
- Investigating the effect different tyre modelling approaches can have on the oscillations.
- Studying the effect on the oscillations with and without the controllers by including viscous damping in the model.
- Improving backlash controller to cut down the lag time and improve the system response.
- Real world testing of the controllers.
- A study on how the performance of the controller will be influenced if the requested torque input was limited by few units below the allowable torque which would in turn allow for effective torque after controller to have few more units to use for control purpose above the requested torque before it reaches the allowable limit.

References

- [1] J. Fredriksson, H. Weiefors and B. Egardt, "Powertrain Control for Active Damping of Driveline Oscillations," *Vehicle System Dynamics*, vol. 37:5, pp. 359-376, 2002.
- [2] M. Menne and O. Bitsche, "Comparison of Drivetrain-Oscillation Damping- Algorithms for Electrical Vehicles," *International Electric Vehicle Symposium*, vol. 18, 2001.
- [3] J. S. Bang, Y.-K. Ko and T.-H. Jung, "The Active Damping Control to Reduce Driveline Oscillations for Electric Vehicles Using Wheel Speeds," *SAE Technical Paper*, 2015-01-1113.
- [4] N. Amann, J. Böcker and F. Prenner, "Active damping of drive train oscillations for an electrically driven vehicle," *IEEE/ASME Transactions on Mechatronics*, vol. 9, pp. 697-700, December 2004.
- [5] C. F. Caruntu, A. E. Balau and C. Lazar, "Cascade based control of a drivetrain with backlash," *Optimization of Electrical and Electronic Equipment (OPTIM) 12th International Conference on*, vol. 12, pp. 710-715, 2010.
- [6] B. Jacobson, *Vehicle Dynamics Compendium for Course MMF062*, Göteborg: Chalmers University of Technology, 2013.
- [7] H. Naunheimer, *Automotive Transmissions*, Second ed., Springer Science, 2011.
- [8] R. Rajamani, *Vehicle Dynamics and Control*, Springer Science, 2006.
- [9] H. B. Pacejka, *Tyre and Vehicle Dynamics*, Second ed., Elsevier, 2006.
- [10] M. Nordin and P.-O. Gutman, "Controlling mechanical systems with backlash - a survey," *Automatica*, vol. 38, no. 10, pp. 1633-1649, October 2002.
- [11] A. Lagerberg, "Control and Estimation of Automotive Powertrains with Backlash," Chalmers University of Technology, Göteborg, 2004.
- [12] R2016a Mathworks Documentation, "http://se.mathworks.com/help/simulink/slref/backlash.html?s_tid=srchtitle," Mathworks, June 2016. [Online].
- [13] S. M. Savaresi and M. Tanelli, *Active Braking Control Systems Design for Vehicles*, Wiesbaden: Springer-Verlag, 2010.
- [14] W. Hernandez, "Improving the Response of a Wheel Speed Sensor by Using a RLS Lattice Algorithm," *Sensors*, vol. 6, pp. 64-79, 2006.
- [15] V. Berbyuk, *Structural Dynamics Control*, Göteborg: Chalmers University of Technology, 2014.
- [16] U. Kiencke and L. Nielsen, *Automotive Control Systems*, Second ed., Springer Science, 2005.
- [17] C. Mo, A. Beaumont and N. Powell, "Active Control of Driveability," *SAE Technical Paper 960046*, 1996.
- [18] J. M. Rodríguez, R. Meneses and J. Orús, "Active vibration control for electric vehicle compliant drivetrains," *Industrial Electronics Society, IECON, 39th Annual Conference of the IEEE*, pp. 2590-2595, 2013.

- [19] P. Templin and B. Egardt, "A Powertrain LQR Torque Compensator with Backlash Handling," *Oil & gas science and technology*, vol. 66(4), pp. 645-654, 2011.
- [20] J. F. Xu, P. Yu, T. Zhang and R. Guo, "Design of Torsional Vibration Controller for Motor-Gearbox/Differential Drive System of Electric Vehicles," *Applied Mechanics and Materials*, vol. 437, pp. 56-61, 2013.

Appendix

Appendix I: Vehicle Parameters

Vehicle Parameters		
Parameters	Value	Units
Vehicle Mass	2200	kg
Horizontal distance from centre of gravity to front axle	1	m
Horizontal distance from centre of gravity to rear axle	2	m
Centre of gravity height	0.65	m
Frontal area	2.252	m ²
Coefficient of drag	0.31	-
Air density	1.2	kg/m ³
Centre of pressure height	0.5	m
Gravitational acceleration	9.8	m/s ²
Motor and Gearbox Parameters		
Maximum power	140	kW
Maximum torque	287	Nm
Maximum speed	12300	RPM
Motor inertia	0.05	kg/m ²
Primary gear inertia	0.005	kg/m ²
Secondary gear inertia	0.005	kg/m ²
Final gear inertia	0.005	kg/m ²
Gear ratio	8.28	-
Powertrain Housing Parameters		
Powertrain housing inertia	1.1	kg/m ²
Powertrain housing mount stiffness	20000	Nm/rad
Powertrain housing mount damping	57	Nm/(rad/s)
Shaft Parameters		

Shaft stiffness per axle	25200	Nm/rad
Shaft damping per axle	0.05	Nm/(rad/s)
Wheel and Tire Parameters		
Wheel inertia per axle	1.2	kg/m ²
Radius of wheel	0.33	m
Longitudinal tire stiffness per axle	14000	N
Rolling resistance coefficient	0.01	-

Appendix II: Simulink Model

